2017

# Nature of Bonding in Bimetallic or Ligated Aluminum Clusters

Cam J. Grover
*Virginia Commonwealth University*

# Nature of Bonding in Bimetallic or Ligated Aluminum Clusters

A thesis submitted in partial fulfillment of the requirements for the degree of Master of Science at Virginia Commonwealth University.

By


Cameron Joseph Grover

B.S Biomedical Engineering, 2013
Virginia Commonwealth University


Director: Dr. Shiv N. Khanna
Commonwealth Professor
Department of Physics

Virginia Commonwealth University
Richmond, Virginia
May 2017

# Acknowledgements

I'd like to first thank Dr. Shiv Khanna of the Physics department at VCU for accepting me into his group not once, but twice. His patience and clarity has served as a model I have sought to reproduce in my own teaching responsibilities. His affability promotes confidence in his students, encourages them to ask questions, and fosters enthusiasm in his pupils.

Next, I'd like to thank Dr Arthur Reber and the other members from the group (esp. Dr. Vikas Chauhan). They taught me how to use the software in this thesis. Whenever I had a problem or question, they would drop whatever there were doing to help me out. Without their help, my experience in research would have been far less fruitful.

I'd like to also thank Dr. Alenka Luzar and Dr Marilyn Bishop for agreeing to serve on my committee.

Finally, I recognize that I would not be where I am without the love and constant support from my friends and family.

# Table of contents

Acknowledgments ..... ii

List of Tables and Figures ..... v

Abstract ..... vii

## Chapter 1. Introduction

1.1 Motivation ..... 1

1.2 Types of bonds ..... 2

1.3 Spherical Jellium Model ..... 3

1.4 Wade-Mingos Counting Rules ..... 4

1.5 Hirshfeld Charge ..... 4

1.6 Mulliken Population ..... 5

1.7 Summary and Thesis Outline ..... 5

## Chapter 2. Theoretical Methods

2.1 Schrodinger's Equation ..... 7

2.2 Density Functional Theory ..... 7

2.3 DFT Software ..... 11

## Chapter 3. Nature of Bonding in Bimetallic Clusters

3.1 Introduction ..... 13

3.2 Geometries ..... 13

3.3 HOMO-LUMO Gaps and Jahn-Teller distortion ..... 19

3.4 Hirshfeld charge and Dipole Moments ..... 23

3.5 Laplacian of Charge Density ..... 26

3.6 Mulliken Population ..... 27

3.7 Change in Removal Energy .....29
3.8 Change in electronic Structure .....30
Chapter 4. Nature of Bonding in Ligated Aluminum Clusters
4.1 Introduction .....35
4.2 Geometries .....36
4.3 HOMO-LUMO Gaps and Removal Energy .....38
4.4 Mulliken Populations .....39
4.5 Electronic Structure .....41
Chapter 5. Conclusion and Future Work
5.1 Conclusions .....46
References .....48

# List of Table and Figure

**Figure 1**. $Al_nMg_m$ – Optimized Geometries .....14

**Figure 2.** $Al_nMg_m^-$ – Optimized Geometries .....15

**Figure 3.** $Al_nNa_m$ – Optimized Geometries .....16

**Figure 4.** $Al_nNa_m^-$ – Optimized Geometries .....17

**Figure 5.** Difference in Average Distance from Center of Mass (Dopant – Aluminum) .....18

**Figure 6.** HOMO-LUMO Gap for $Al_nMg_m^-$ .....19

**Figure 7.** Electronic Structure of $Al_5Mg_2^-$, $Al_{11}Mg_3^-$, and $Al_{13}^-$ .....20

**Figure 8.** Electronic Structure of $Al_7Mg_3^-$, and $Al_9^-$ .....21

**Figure 9.** Electronic Structure of $Al_{11}Mg^-$, $Al_{11}Mg_2^-$, and $Al_{13}^+$ .....22

**Figure 10.** Hirshfeld Charge and Dipole Moment .....24

**Figure 11.** Dipole Moment of Bimetallic with Multiple Dopants .....25

**Figure 12.** $Al_{13}Mg$ Hirshfeld Charge .....26

**Table 1.** Laplacian of Charge Density at different Critical Points .....27

**Figure 13.** Dopant Mulliken Population for $Al_nX_m$ (X = Na and Mg) .....28

**Figure 14.** Change in Dopant Removal Energy between Anion and Neutral .....30

**Figure 15.** Electronic Structure of optimized $Al_{12}Na^-$, optimized $Al_{12}^{2-}$, single point calculation $Al_{12}^{2-}$ with geometry from $Al_{12}Na^-$ .....31

**Figure 16.** Electronic Structure of optimized $Al_{12}Na_3^-$, optimized $Al_{12}^{4-}$, single point calculation $Al_{12}^{4-}$ with geometry from $Al_{12}Na_3^-$ .....32

**Figure 17.** Electronic Structure of optimized $Al_{11}Mg_3^-$, optimized $Al_{12}^{7-}$, single point calculation $Al_{11}^{7-}$ with geometry from $Al_{11}Mg_3^-$ .....33

**Figure 18.** Optimized Geometries of Ligated Aluminum Clusters .....37

**Figure 19.** HOMO-LUMO Gaps of Ligated Aluminum Clusters .....38

**Figure 20.** Removal Energy of Ligated Aluminum Clusters .....39

**Figure 21.** Mulliken Population of Pure and Ligated $Al_n$ clusters .....40

**Figure 22.** Electronic Structure of $K_2(AlMethyl)_n$ $(3 \leq n \leq 12)$ .....41

**Figure 23.** Electronic Structure of $K_2(AlMethyl)_4$ and $K_2(AlMethyl)_{12}$ .....43

# Abstract

NATURE OF BONDING IN BIMETALLIC AND LIGATED ALUMINUM CLUSTERS

By: Cameron Joseph Grover

A thesis submitted in partial fulfillment of the requirements for the degree of Master of Science at Virginia Commonwealth University.

Virginia Commonwealth University, 2017

Major Director: Dr Shiv N. Khanna, Commonwealth Professor, Physics Department

In this study, Amsterdam Density Functional software is used to model bimetallic and ligated aluminum clusters. The stability of the bimetallic clusters is well described by the Jellium model, and the nature of bonding between dopants and aluminum in the bimetallic clusters is analyzed using different criteria. We find that sodium tends to bind ionically, while the bonding of magnesium is not so obvious. We also determine that examining the Mulliken population is the most useful parameter in differentiating bonding character. Calculations on ligated aluminum clusters reveal it behaves fundamentally different than the bimetallic clusters studied in the first part. The ligated clusters contained a high HOMO-LUMO gap regardless of size and the aluminum showed a high 3*p* Mulliken population. These results show ligated aluminum clusters behave according to Wade-Mingos counting rules.

# Chapter 1
# Introduction

## 1.1 Motivation

Advances in the last several decades have provided the prospect for a new class of solids: cluster assembled material. The constituents of this class of solid would be individual atomic clusters that agglomerate into a larger structure while maintaining their identity[1–9]. In contrast to bulk materials where properties are independent of size, the properties of clusters vary with the number of atoms[10–14]. One such example of this is aluminum. Bulk Al readily oxidizes while experiments indicate that $Al_{13}^-$, $Al_{23}^-$, etc. are resistant to etching by oxygen[6]. Computational investigations show $Al_{13}^-$ possess a large gap between the highest occupied molecular orbital (HOMO) and the lowest unoccupied molecular orbital (LUMO) due to an electronic shell closure at 40 valence electrons[14]. These results illustrate that $Al_{13}^-$ has different chemical properties than bulk aluminum, which readily forms an oxide layer[6,14]. This dependence of properties on size provides a mechanism to create novel building blocks. For example, it has been shown that $As_7$ clusters can be used to create a crystal in conjunction with alkali metals that donate electrons[2,3,7,15]. By changing the counter-cations, the band gap of the material can be varied between 1.1 eV and 2.1 eV[15]. The cluster materials combine intra-cluster and inter-cluster interactions and therefore offer an additional control via these interactions.

This study will deal with two aspects of these cluster assembled materials. Principally, the bonding in clusters will be examined. The bonding among the atoms within a cluster will govern the nature of electronic shells and if and how that cluster will agglomerate into a crystal. The bonding among the atoms will also determine which electron counting rules can be used to understand the stability of the system[16–19]. The Jellium model, where the electrons respond to a uniform positive background, has been extensively used to describe metallic systems[16,17]. Alternatively, covalently bonded systems are best described by Wade-Mingos counting rules[18,19].

## 1.2 Types of bonds

The bonds between atoms lead to different electronic properties[20,21]. Metallic bonds involve a delocalized electron cloud in the lattice of ionic cores[22]. These systems have a finite density of states at the Fermi energy, which leads to electrical conduction. This property allows the electrons to respond to an external electric field, quenching any dipole moments.

Ionic bonds involve electronic transfer from a cation to an anion. This bond is stabilized by the coulombic interaction between the positively charged cation and negatively charged anion. It has been shown that this type of interaction can lead to structure-seeking behavior in the development of cluster-assembled materials[2,15].

Covalent bonding occurs when electrons are shared by more than one atom. In semiconductors, this bonding leads to a gap between the occupied and unoccupied states, resulting in a strong dependence of conductivity on temperature or impurities. Boron clusters tend to form planar structures that are stabilized by aromaticity[23,24]. This aromaticity comes about from the overlap

of atomic p-orbitals above and below the plane containing the atoms of some molecule. These orbitals become continuous and form delocalized electron clouds above and below the plane of the atoms[23,24].

### 1.3 Spherical Jellium Model

The difference among these bonding types is not as clear when we shift from bulk materials to clusters containing less than a few hundred atoms. The Jellium Model, used to describe metallic systems, assumes that the net charge of the positive ionic cores is smeared continuously across space, leading to a picture similar to the spherical potential well[25]. In this model, allowed energy states for the electrons of the cluster are grouped into shells similar to that of an individual atom[25]. It is important to note that only valence electrons are free to move in this model; the core electrons stay associated with their ionic cores.

As certain shells become filled with these valence electrons, there exists a large HOMO-LUMO Gap. The valence electron counts that correspond to a filling of these shells are referred to as "magic numbers" (2, 8, 18, 20, 34, 40, etc…), which lead to enhanced stability, higher ionization potential, and lower polarizability[14,26].

This model is metallic in nature; the valence orbitals are spread over multiple atoms are are confined by a uniform positive background charge distribution. As such, this model is often invoked to describe metallic clusters.

## 1.4 Wade-Mingos counting rules

If the molecular orbitals are more localized along different directions, a different set of "magic numbers" occurs. Wade-Mingos counting rules predict the structure of a cluster based on the number of available pairs of electrons for bonding. In this model, the individual units will form a skeletal cage whose geometry will depend on the number of skeletal bonding pairs. The prediction is that a species containing *n* atoms and has (*n*+1) pairs of electrons available for bonding will have a *closo*-structure. A species having (*n*+2) and (*n*+3) pairs of electrons available for bonding will have *nido*- and *arachno*- structures, respectively[18,19].

An example: In the dodecaborane molecule ($B_{12}H_{12}^{2-}$), each B-H unit contains two electron pairs. One of these electron pairs bonds the boron to the hydrogen, while the other is available for cluster bonding. The total number of electron pairs is therefore *n*+1, and Wade-Mingos rules accurately predict a stable, cage-like, *closo*-structure. Furthermore, any cluster of the form $B_nH_n^{2-}$ will have a high HOMO-LUMO gap and take on a cage structure. This is a fundamentally different behavior from the Jellium model where a high HOMO-LUMO gap is only possible in clusters with specific numbers of electrons.

## 1.5 Hirshfeld Charge

Our objective is to determine whether a dopant binds metallically or ionically to the aluminum cluster. The most straightforward way to investigate this behavior is to look at the Hirshfeld Charge. For this calculation, the charge density at a point is shared by all atoms and compared to

the free-atom charge density at the corresponding distances from the nuclei[27]. Integrating across space allows the program to determine the total net atomic charges for each of the constituent atoms in a cluster, where the atomic charges are reported as fractions of the elementary charge[27].

## 1.6 Mulliken Population

Density function theory models a molecular orbital as the linear combination of atomic orbitals. Mulliken population is calculated from the coefficients of this linear combination[28]. As a note, the atomic orbitals will be denoted as lower case (*s*, *p*, *d*), while the molecular orbitals will be denoted with capital letters (S, P, D). From this Mulliken population, the occupation of the atomic orbitals is compared to that of the free atom, and a net charge is calculated. It is important to note Mulliken population is heavily dependent on the basis set chosen; different basis will lead to different coefficients in wave function expansion. It is for this reason that atomic charges based on a Mulliken are less reliable than the Hirshfeld charge analysis.

## 1.7 Summary and Outline

The goal of this thesis is to investigate the nature of bonding in bimetallic and ligated aluminum clusters. The Amsterdam Density Functional software is used to calculate the electronic structures for each cluster. Chapter 2 contains a brief overview of the density functional theory and the approximations that make calculations feasible. The research completed for this thesis

are found in the following two chapters. In Chapter 3, we will model aluminum clusters doped with magnesium or sodium. In Chapter 4, we will model aluminum-methyl clusters with two potassium counter ions. Chapter 6 will contain conclusions and future work.

# Chapter 2

# Theoretical Methods

## 2.1 Schrodinger Equation

Schrodinger's equation is an eigenvalue equation that has become ubiquitous in describing quantum mechanical systems. The time independent form of this equation serves as the foundation of the algorithms used in this study. This formulation is

$$\hat{H}\,\Psi = E\Psi$$

## 2.2 Density Functional Theory (DFT)

Density function theory (DFT) is a computational modeling framework that numerically approximates the Hamiltonian and optimizes the wave function of the electrons through a self-consistency algorithm. This framework makes several approximations along the way. The

complete Hamiltonian describing the nuclei and electrons of some atomic system can be found below.

$$\hat{H} = -\sum_{n=1}^{N} \frac{\hbar^2}{2\,m_e} \nabla_n{}^2 - \sum_{m=1}^{M} \frac{\hbar^2}{2\,m_n} \nabla_m{}^2 - \sum_{i=1}^{N}\sum_{j=1}^{M} \frac{Z_j\,e^2}{r_{ij}} - \sum_{\alpha=1}^{N}\sum_{\beta>\alpha}^{N} \frac{e^2}{r_{\alpha\beta}} + \sum_{A=1}^{M}\sum_{B>A}^{M} \frac{Z_A\,Z_B\,e^2}{r_{AB}}$$

The first terms in the Hamiltonian refers to the kinetic energy of *N* electrons with mass $m_e$, while the second term refers to the kinetic energy of *M* nuclei with mass $m_n$. The third term is the potential between the electrons and the nuclei, where *e* is the charge of an electron, $Z_j$ is the atomic number of the nucleus and $r_{ij}$ is the distance between a nucleus and an electron. The fourth term refers to the potential energy of all the electrons where $r_{\alpha\beta}$ is the distance between electrons. The fifth term is the potential energy of all the nuclei. $Z_A$ and $Z_B$ are the atomic numbers of the nuclei and $r_{AB}$ is the distance between the two nuclei.

The Born-Oppenheimer approximation treats the Hamiltonian and wave-functions of the nuclei and electrons independently. This is possible because the mass of the electrons is orders of magnitude less than that of the nuclei. Therefore, the ionic cores can be considered to be stationary with respect to the electrons. With this approximation, we can separate the electronic and nuclear degrees of freedom and omit the second and fifth terms of the previous Hamiltonian to describe only the electrons. This new electronic Hamiltonian is

$$\hat{H}_e = -\sum_{n=1}^{N} \frac{\hbar^2}{2\,m_e} \nabla_n{}^2 - \sum_{i=1}^{N}\sum_{j=1}^{M} \frac{Z_j\,e^2}{r_{ij}} - \sum_{\alpha=1}^{N}\sum_{\beta>\alpha}^{N} \frac{e^2}{r_{\alpha\beta}}$$

We can convert this function to atomic units where the mass and charge of the electron are unity.

$$\hat{H}_e = -\sum_{n=1}^{N} \frac{1}{2} \nabla_n^2 - \sum_{i=1}^{N} \sum_{j=1}^{M} \frac{Z_j}{r_{ij}} - \sum_{\alpha=1}^{N} \sum_{\beta>1}^{N} \frac{1}{r_{\alpha\beta}}$$

The eigenvalues from this operator will give the energy levels of the electrons. The total energy of the system will be these electronic energies and the energies from the nuclei. That is

$$\hat{H}_e \Psi_e = E_e \Psi_e \quad \text{and}$$
$$E_{\text{total}} = E_e + E_{\text{nuclear}}$$

We can further simplify this Hamiltonian by approximating the potential among electrons with a mean field. This is where density functional theory gets its name: the potential energy becomes a function of the electron density (which is defined by the wave function). The Hatree Fock method for solving this problem involves expressing the wavefunction as a product of the one electron functions.

$$\Psi^{\text{HF}} = \prod_{i=1}^{N} \phi_i(\vec{r}_i)$$

The electrons influence each other not just through a mutual coulombic repulsion, but also through correlation and exchange effects. Within the density function theory framework, the interacting electron system is replaced by a non-interacting gas where the exchange and correlation effects are modeled with the gradient corrected density functionals developed by Perdew et al[29]. Other functionals have been proposed, but the functional used in this study has been shown to accurately model the electronic structures of $Al_n$, $Mg_n$, $Na_n$, as well as $Al_nMg_m$

clusters[10,11,30,31]. The equation to be solved is called the Kohn-Sham equation, which deals with charge density instead of the one electron functionals.

$$\left(-\frac{\hbar^2}{2m}\nabla^2 + V_{\text{ext}}(\vec{r}) + V_H(\rho) + V_{\text{XC}}(\rho)\right)\Psi = \varepsilon_i \Psi$$

Here, $V_{ext}$ refers to the potential among the electrons and the ionic cores, $V_H$ refers to the potential among the electrons, and $V_{XC}$ corrects for quantum mechanical effects associated with the exchange and correlation among electrons. This discussion has set up what equation will be solved, but not how it will be solved. As a reminder, the potential energy term in the operator is dependent on the charge density of the electron, and therefore its wavefunction. The electron density is related to the one electron wave function via the relation:

$$\rho(\vec{r}) = \sum_{i}^{N} n_i |\phi_i(\vec{r})|^2$$

The wavefunction is a linear combination of atomic orbitals centered at the atomic sites.

$$\Psi = \sum C_n \phi_n$$

These atomic orbitals, $\phi_n$, making up the wavefunction are referred to as the basis. Two common functions used to model quantum confined systems are Gaussians and Slater Type Orbitals. This functional form decays exponentially and has a cusp at the nuclei, making it a better model than a Gaussian function. The program guesses initial values for the coefficients in the wave function expansion. This wave function is used to generate the initial density in the Kohn Sham equations.

At this point, the Schrodinger equation is solved for the energy. The coefficients of the wave function expansion are then changed to satisfy the equality in Schrodinger's equation. A new charge density is calculated from this new wave function for a new Fock Operator. Schrodinger's equation is again solved with the new wave function and new Fock operator to find a new energy. The coefficients are changed again to satisfy the equality, process is repeated until the change in energy is less than a user specified value. The ground state energy is given by

$$E_0 = T(\rho) + \int_V V_{\text{ext}}(\vec{r})\,\rho(\vec{r}) + V_H(\rho) + V_{\text{XC}}(\rho)$$

In addition to energy, the forces on the atoms are also calculated. Once the wave function is optimized, the nuclei are moved a small interval down the potential gradient, and the procedure is run again to calculate the electronic energy. The total energy of the system is again calculated in the new geometry. This geometry optimization continues until the change in energy is below some user specified value. At this point in the algorithm, the system will be described by a wavefunction that is dependent on the chosen basis.

### 2.3 DFT Software

In this study, Amsterdam Density Functional (ADF) was used to complete all DFT calculations[32]. The electron orbitals are represented by Slater Type Orbitals (STO) located at the atomic sites[33]. The general form of STO is

$$\phi(r) = Y_{\ell,m}(\theta, \varphi) r^n e^{-\alpha r}$$

.

In this function, the $Y_{,l,m}(\theta,\varphi)$ factor refers to spherical harmonics, $r$ is the distance from the atomic nuclei, $n$ is the principle quantum number, and $\alpha$ controls the long-range decay. These

orbitals are more suitable than Gaussian Type Orbitals because they contain a cusp at the atomic site as well as possessing a more accurate long distance decay. The basis set used for all calculations was the T2ZP.

In the bimetallic study, up to fifteen different geometries were optimized to provide a large sample of configuration space. In the ligand study, up to five geometries for each species were optimized. These geometries corresponding to different skeletal structures as well as different placements for the cations. In both studies, various spin multiplicities were tried to ascertain the multiplicity of the ground state. For both geometric optimizations, the convergence threshold was $10^{-8}$ Hartree. In the bimetallic study, the Hirshfeld charge and Mulliken populations were analyzed[27,28]. The molecular orbitals were viewed in ADF viewer and classified based on the number of nodes and the symmetry of the wave function.

# Chapter 3

# Nature of Bonding in Bimetallic Clusters

## 3.1 Introduction

The objective of this chapter is to investigate the nature of bonding between dopants and an aluminum cluster using. The bonding in pure $Al_n$ clusters is metallic and can be reasonable described by a confined nearly free electron gas. Our objective is to examine the nature of bonding between aluminum clusters and Na or Mg dopants. The obvious starting point in making this distinction is to analyze the Hirshfeld charge and Dipole moments. We go on to analyze the 3s and 3p Mulliken populations of the dopants, as well as the Laplacian of the charge density at critical points. The change in dopant removal energy between anionic and neutral species is calculated. Finally, we determine if the electronic structure is dramatically changed by replacing the dopants with their corresponding valence electrons. By analyzing a broad range of parameters, we hope not to just distinguish between metallic and ionic bonding, but to find the parameter which would be most useful in differentiating metallic and ionic bonding.

## 3.2 Geometries

First, we look at the structures of the magnesium or sodium doped aluminum clusters. Figure 1 shows the neutral structures of $Al_nMg_m$, and Figure 2 shows the corresponding anionic structures. In these, aluminum is shown as the gray atoms, and magnesium as the green. The connections between the atoms are to help illustrate the structures of the clusters and do not represent bonds Some characteristic bond lengths are included.

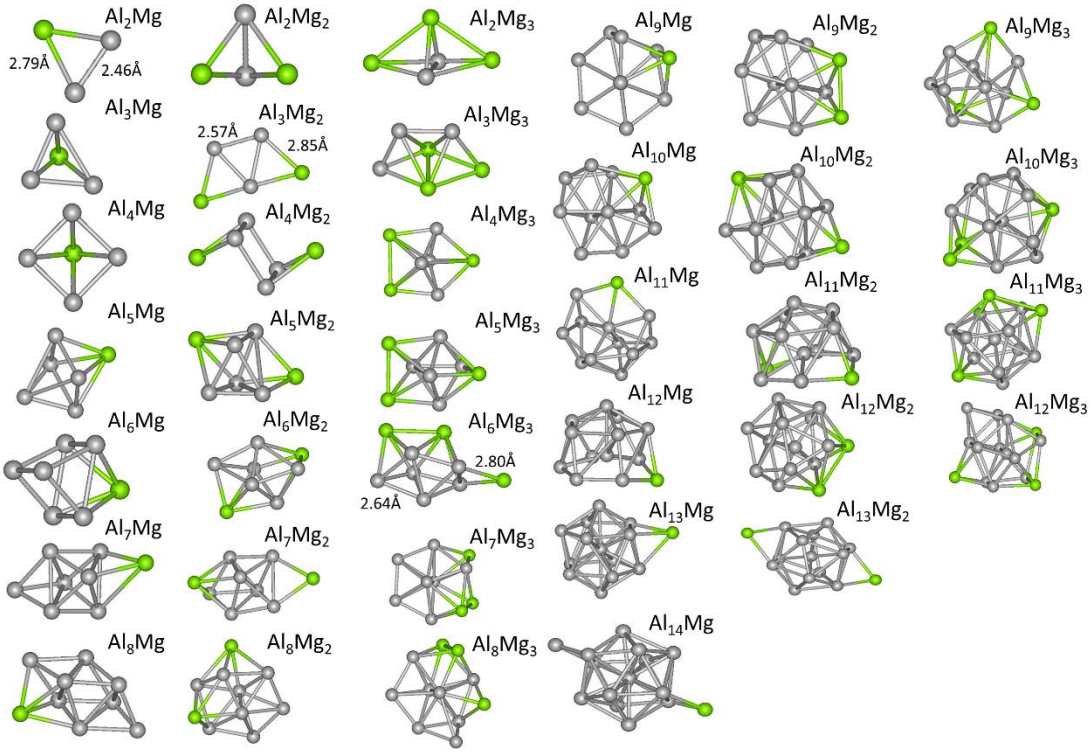


*Figure 1 - Aluminum Magnesium cluster structures - Neutral*

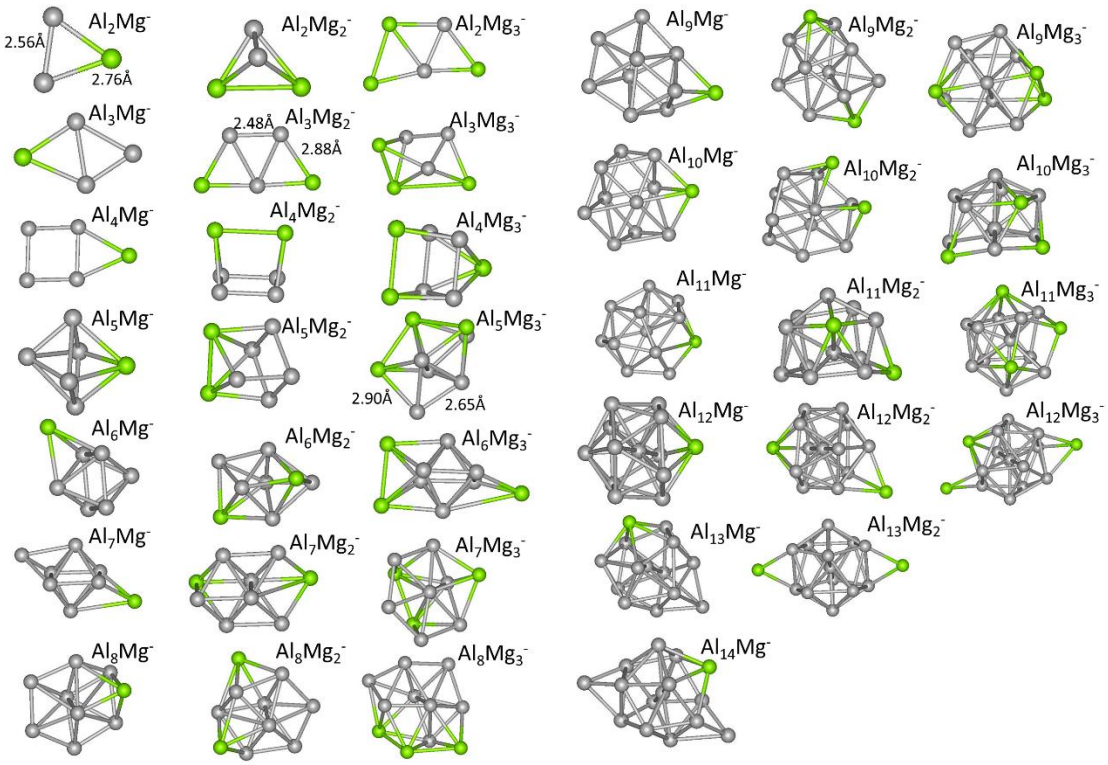


*Figure 2 - Aluminum magnesium cluster structure - anion*

Figures 3 and 4 show the neutral and anionic structures of $Al_nNa_m$, respectively. Here aluminum is shown in gray, while sodium is purple. Again, the lines connecting the atoms are to help illustrate the structure of the clusters and do not represent bonds, and some characteristic bond lengths are included.

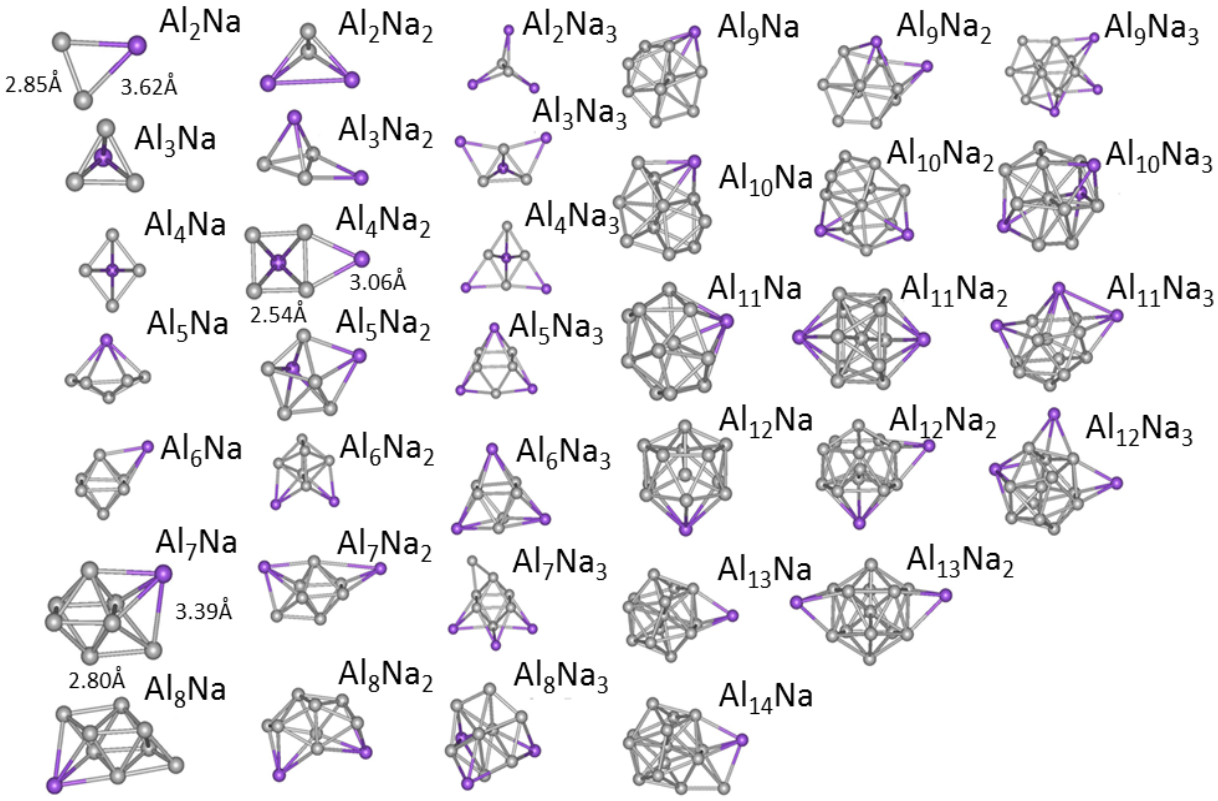


*Figure 3 -Aluminum-Sodium cluster structures - Neutral*

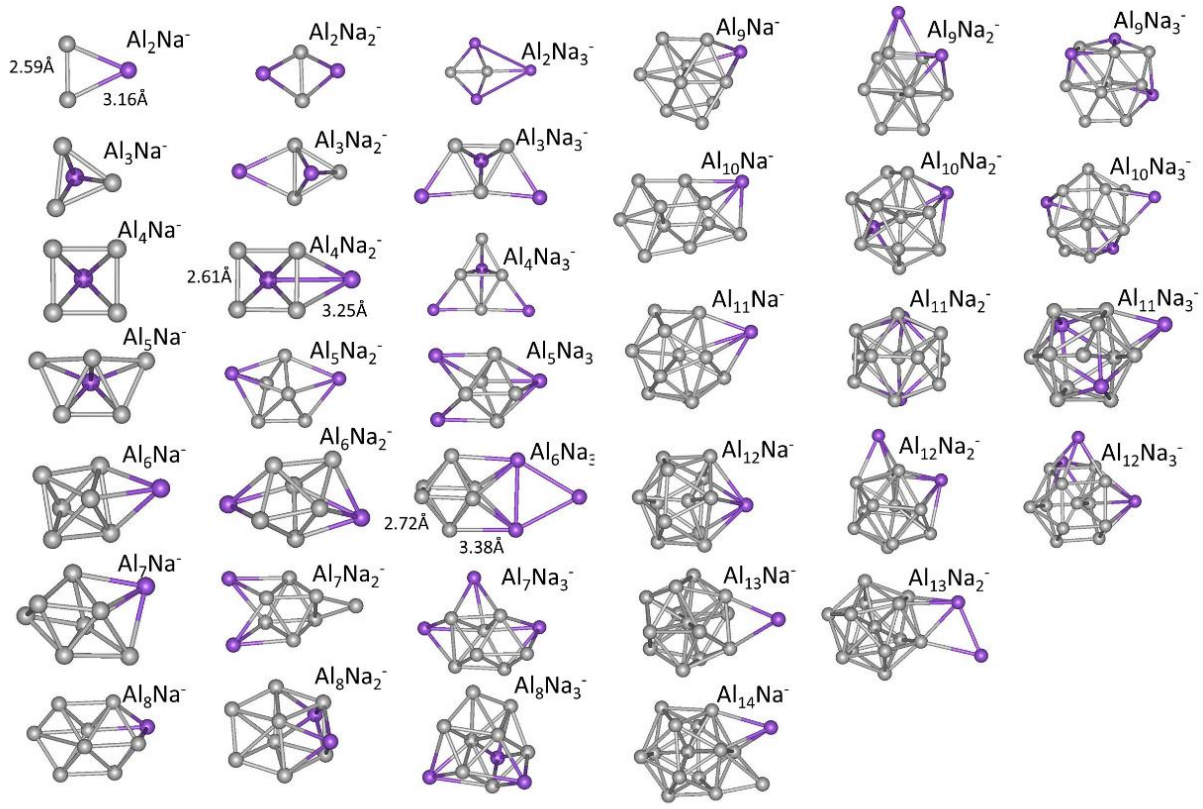


*Figure 4 - Aluminum-Sodium cluster structures - Anions*

It can be observed that the dopants (magnesium or sodium) tend not to bind to each other, but instead prefer bonding with the aluminum motif. This can be explained by considering the bond strengths of the dimers. Al-Mg (0.53eV) and Al-Na (0.90eV) bond strengths are stronger than the Na-Na (0.54eV) or the Mg-Mg(0.10eV) bond strengths, while Al-Al (1.18eV) are the strongest. Additionally, aluminum-magnesium bonds tend to be shorter than the aluminum-sodium bonds.

Another difference between the two types of systems is that the magnesium tends to embed itself within the aluminum motif, while sodium tends to bind to the outside. In order to quantify this trend, we find the average distance of the dopants from the center of mass and the average distance of the aluminum from the center of mass. The difference between these two average

distances is plotted as a function of cluster size for both the neutral and anionic structures. This quantity shows how much further the dopant is than the aluminum from the center of mass; a positive value corresponds to the dopant being further than the aluminum. Figure 5 shows this difference as a function of size. The six traces correspond to different numbers of dopants. Sodium is represented with red and magnesium with blue. The darkness of the trace corresponds to number of dopants (i.e. dark blue has more magnesium than light blue).

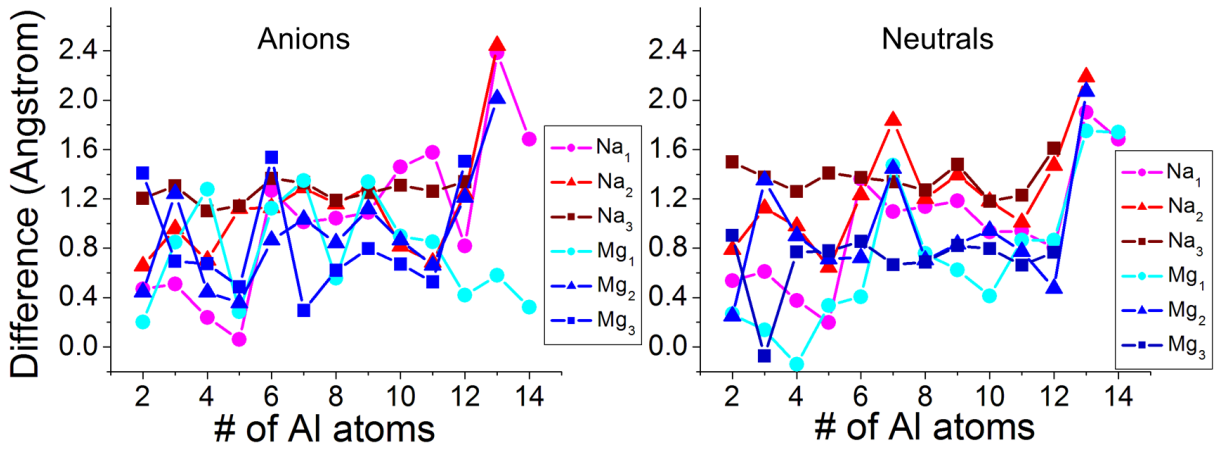


*Figure 5 – Average difference in distance between dopant and aluminum in anion and neutral series*

In these clusters, magnesium and sodium both tend to be further from the center of mass than the aluminum atoms. In clusters containing seven to twelve atoms, sodium tends to be further from the center of mass than magnesium with respect to the aluminum atoms. In clusters containing at least thirteen aluminum atoms, a sharp increase is seen for both magnesium and sodium clusters. This because $Al_{13}$ tends to form into an icosahedron, with the dopants binding to the outside. This behavior is what we would expect from an ionic system: the aluminum atoms form a compact cluster to which the cations are ionically bound.

### 3.3 HOMO-LUMO Gaps and Jahn-Teller Distortion

Figure 6 shows the HOMO-LUMO gaps of $Al_nMg_m^-$ as a function of the number of valence electrons. Our results show that a high HOMO-LUMO gap (>1.0eV), can occur in clusters not possessing a "magic number" of electrons. To find the number of valence electrons, we considered each aluminum atom to contribute three electrons, while each magnesium would contribute two. Again, each trace corresponds to different number of magnesium atoms, with $Mg_0$ representing a pure aluminum cluster.

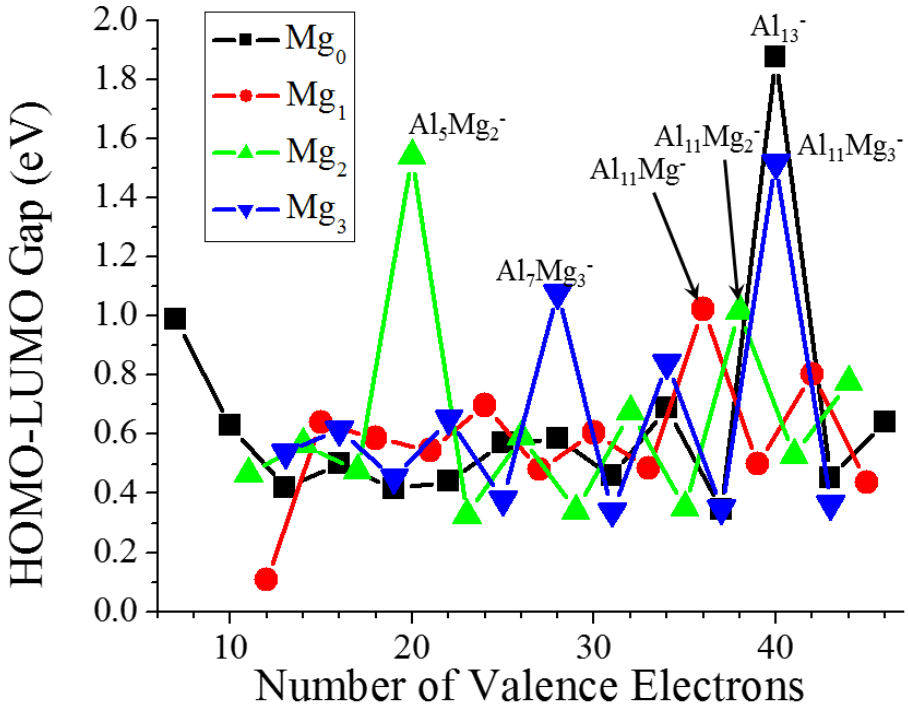


*Figure 6 - HOMO-LUMO gaps: Aluminum Magnesium Anions*

Five species were found to have HOMO-LUMO gaps greater than 1.0eV: $Al_5Mg_2^-$, $Al_7Mg_3^-$, $Al_{11}Mg^-$, $Al_{11}Mg_2^-$, and $Al_{11}Mg_3^-$. The stability of $Al_5Mg_2^-$ and $Al_{11}Mg_3^-$, which possess 20 and 40 valence electrons, are predicted by the Jellium model; we have to consider another effect to

explain the stability of the other species. $Al_7Mg_3^-$, $Al_{11}Mg^-$, and $Al_{11}Mg_2^-$ have 28, 36, and 38 valence electrons respectively. The origin of these unexpected stabilities was investigated by analyzing the molecular orbitals to get a clearer view of the electronic structure of each. To start, we look at the electronic structure $Al_5Mg_2^-$, $Al_{11}Mg_3^-$, and $Al_{13}^-$, whose stability can be explained with the Jellium Model. Figure 7 shows the electronic structures of these three species. The orbital shapes were visualized and assigned a shell designation based on the number and shape of the nodes. A representative orbital from each shell is displayed alongside that shell.

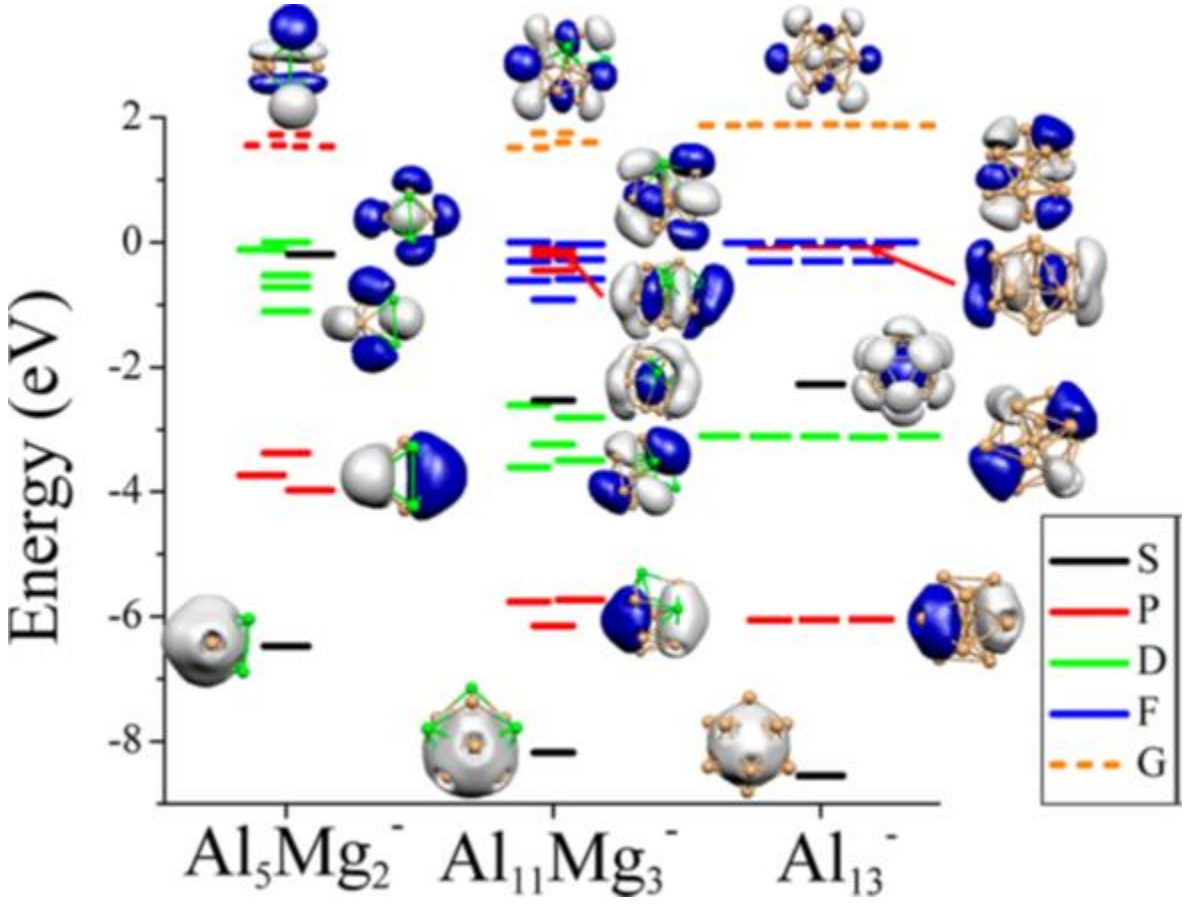


*Figure 7 - Electronic Structure of $Al_5Mg_2^-$ (20 $e^-$), $Al_{11}Mg_3^-$ (40$e^-$), and $Al_{13}^-$ (40$e^-$)*

There is little breaking of the degeneracy of the molecular orbitals within the individual subshells. That is, the energies of a particular subshell closely match those of the same assignment. As the cluster becomes more spherical and more symmetrical, the degeneracy of

these subshells increases. The orbitals of the P and D subshells are completely degenerate in the $Al_{13}^-$ cluster, and there is only a small gap in the F orbitals. This shows that geometric asymmetry can cause the orbitals within an individual subshell to lose their degeneracy, leading to crystal field splitting. This effect is highlighted in $Al_7Mg_3^-$.

From Figure 4, we can see that $Al_7Mg_3^-$ has a much higher HOMO-LUMO gap than $Al_9^-$, in spite of having the same number of valence electrons. The electronic structure of these clusters can be found in Figure 8. In this plot the occupied P and F orbitals are shown

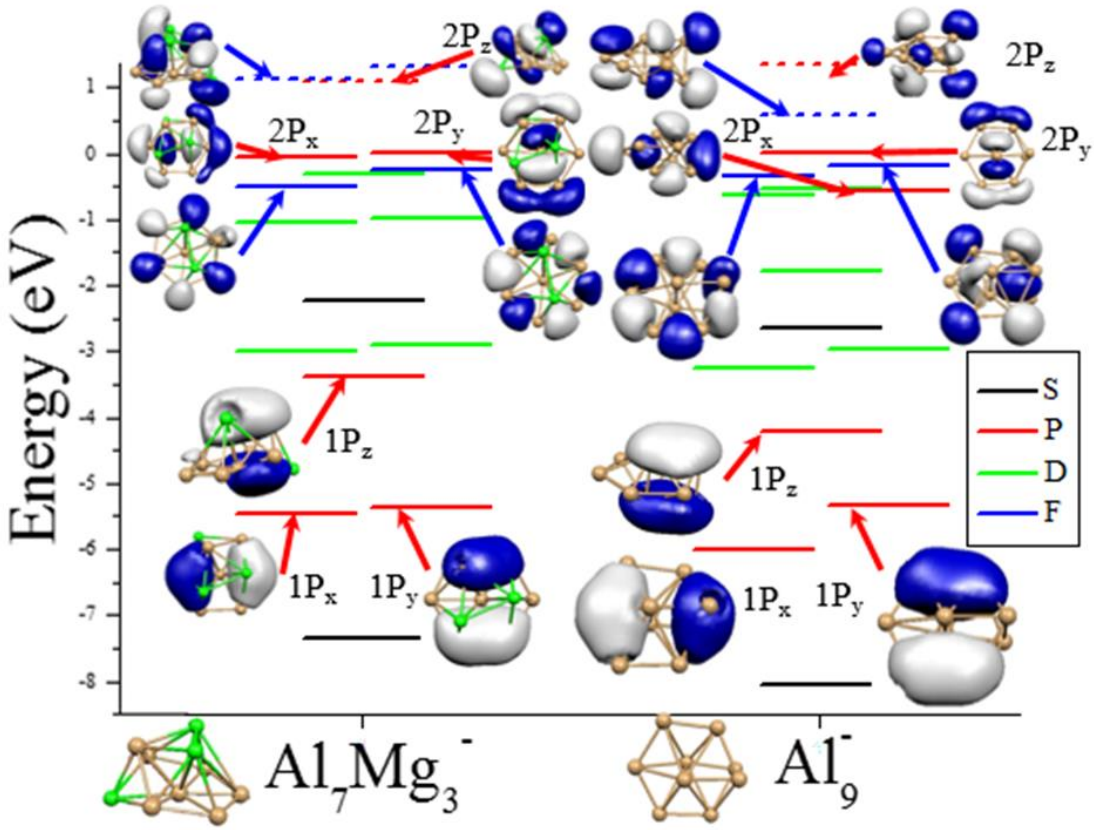


*Figure 8 - Electronic Structure of $Al_7Mg_3^-$ ($28e^-$) and $A_9^-$ ($28e^-$)*

Both $Al_7Mg_3^-$ and $Al_9^-$ have oblate structure. That is, they are compressed in one direction and stretched in the other two. We label the compressed direction *z*, and the other two directions *x* and *y*. The splitting in the molecular P-orbitals emphasizes the effect of this asymmetry on the

energies of the molecular orbitals. For both P subshells, the orbital corresponding to the direction in which the cluster is compressed is higher in energy. The two P orbitals that are relatively lower in energy are assigned $P_x$ and $P_y$, while the orbital that is higher in energy is assigned $P_z$. In the case of $Al_9^-$, this crystal field splitting also causes an unoccupied F orbital to be pushed down in energy, reducing the HOMO-LUMO gap. This demonstrates that orbitals corresponding to a direction that is stretched become more energetically favorable while orbitals corresponding to a direction that is compressed become higher in energy.

The clusters $Al_{11}Mg^-$ and $Al_{11}Mg_2^-$ were also found to have high HOMO-LUMO gaps with electron counts of 36 and 38, respectively. The electronic structures of these clusters are compared with $Al_{13}^+$, which also has a high HOMO-LUMO gap with 38 electrons. Figure 9 shows this comparison.

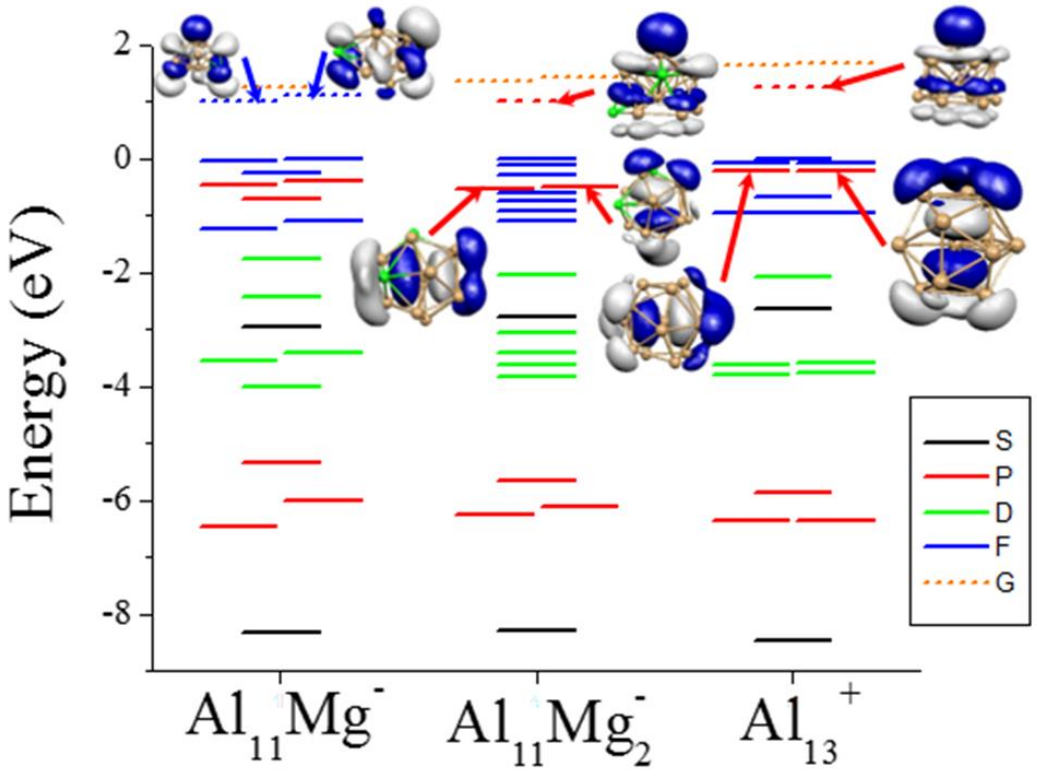


*Figure 9 - Electronic Structure of $Al_{11}Mg^-$ ($36e^-$), $Al_{11}Mg_2^-$ ($38e^-$), and $Al_{13}^+$ ($38e^-$)*

$Al_{13}^+$ is known to have a high HOMO-LUMO gap. Its oblate structure causes a splitting in the 2P subshell, similar to $Al_7Mg_3^-$ and $Al_9^-$. $Al_{11}Mg_2^-$, also possessing an oblate structure, has a very similar electronic structure to $Al_{13}^+$. Its F subshell has less degeneracy, but its high HOMO-LUMO gap comes from its $P_z$ orbital being pushed up in energy. The high HOMO-LUMO gap in $Al_{11}Mg^-$ is caused not from the splitting of the P subshell, but a splitting of the F subshell. Two F orbitals are pushed up in energy, effecting a large HOMO-LUMO gap. These results demonstrate that oblate structures can have a high HOMO-LUMO gap with a few less electrons than those predicted by the Jellium Model.

With a high HOMO-LUMO gap, a cluster is resistant to oxygen, and could make for a useful constituent in a cluster assembled material. However, the bonding nature among the individual atoms within a cluster will determine how the cluster binds to other clusters. In the following sections, the bonding nature of sodium or magnesium to aluminum clusters is investigated.

### 3.4 Hirshfeld Charge and Dipole Moment

The simplest way to ascertain the nature of bonding within a cluster is through the charge density. An atom becoming positively or negatively charged represents a loss or gain of electrons and is indicative of ionic bonding. This separation of charge would lead to a dipole moment. In this section, we analyze the Hirshfeld charge and dipole moments. If a cluster is metallically bound, we would expect to see negligible Hirshfeld charges (all atoms would be electronically neutral) and dipole moments. In an ideal ionic system, there would be complete charge transfer from the cation to the anion. However, in a simple calculation modeling sodium chloride, we

find a calculated charge transfer of 0.65 $e^-$. This shows that calculations on an ideal ionic system will not necessarily display complete charge transfer.

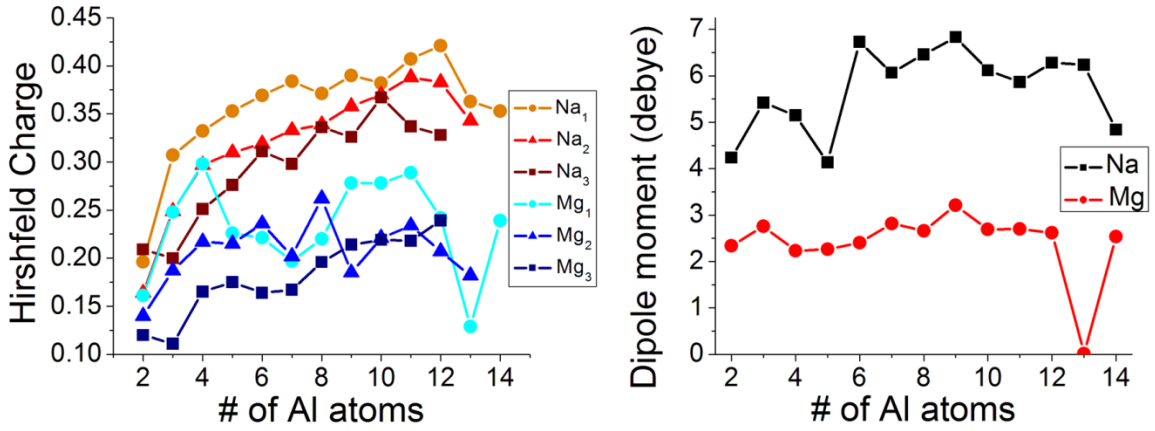


*Figure 10 - Average Hirshfeld Charge of $Al_nNa_m$, and $Al_nMg_m$, and Electric Dipole of $Al_nNa$, and $Al_nMg$.*

Both the calculated Hirschfeld charge and the dipole moments, shown in Figure 10, suggest that magnesium acts as a much weaker cation than sodium. In clusters containing five or more aluminum atoms, the average net charge on the sodium dopants (0.30 – 0.43 $e^-$) is consistently greater than the average net charge on the magnesium dopants (0.10 – 0.27 $e^-$). Figure 11 shows the dipole moment plotted against the number of aluminum atoms in a cluster. Again, red is sodium and blue is magnesium, with darker colors correspond for a higher proportion of the dopant

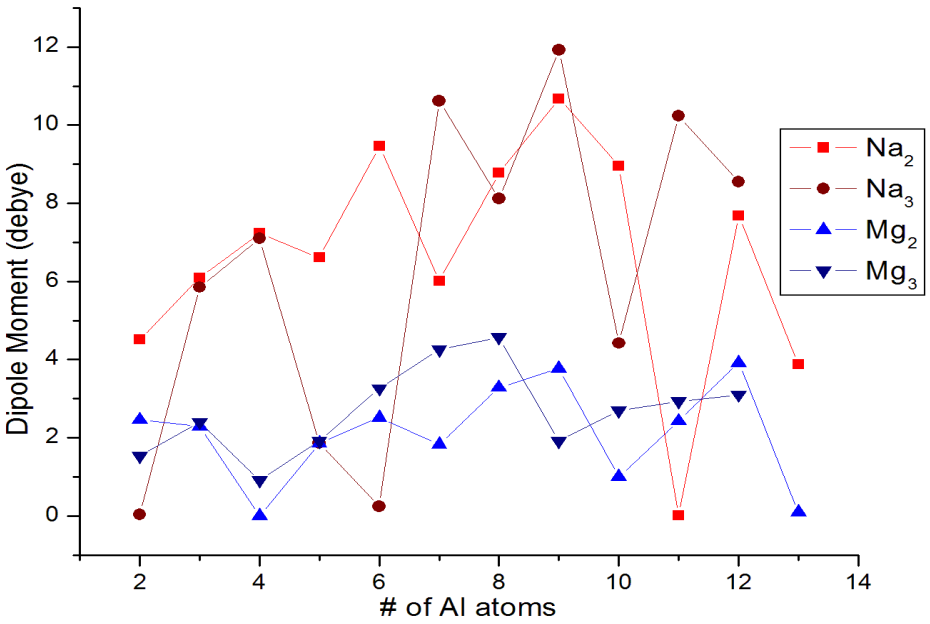


*Figure 11 - Electric Dipole for multiple dopants*

Following the same trend as the Hirshfeld charge, the dipole moment for clusters containing sodium tends to be greater than the dipole moment in clusters containing magnesium. Two clusters have a very low calculated dipole moment $Al_{13}Mg$ and $Al_{11}Na_2$. As shown in Figure 2, the two sodium atoms in $Al_{11}Na_2$ are on opposite sides of the $Al_{11}$ structure. Even though each sodium atom donates charge to the aluminum motif, the geometry causes the net dipole moment to be zero. This shows that distinguishing between ionic and metallic bonding is not as simple as looking at the dipole moment.

The small dipole in $Al_{13}Mg$ can be explained by looking at the charge density across the cluster. Figure 12 shows the Hirshfeld charge at each of the atomic sites.

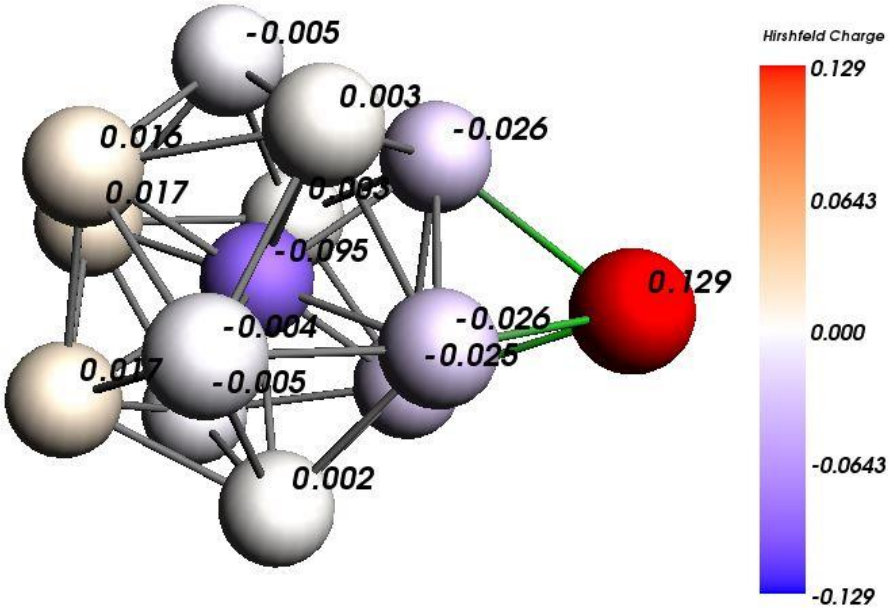


*Figure 12 - $Al_{13}Mg$ Hirshfeld charge*

The magnesium has a positive charge of $0.129e^-$, the neighboring aluminum atoms are slight negative, and the aluminum atoms on the opposite side of the cluster are positively charged. These results demonstrate the polarizability of the $Al_{13}$ motif. With 41 valence electrons, this cluster has an open electronic shell. This single extra electron acts to screen the dipole arising from the weak polar bond between the magnesium and the aluminum motif. This screening is what quenches the electric dipole. These results show that some other metric is needed to distinguish between metallic and ionic bonding.

### 3.5 Laplacian of the Charge Density

The Laplacian of the charge density has been used to characterize ionic versus metallic bonding at bond critical points. A positive Laplacian is indicative of charge depletion and characterizes an

ionic bond, while a negative Laplacian indicates charge accumulation and represents a covalent bond. We sampled the Laplacian of the charge density at different critical points in different clusters. These values can be found in Table 1.

| | Al-Al (Interior) | Al-Al (Exterior) | Al-X |
|---|---|---|---|
| $Al_{13}^-$ | -0.008 | +0.0065 | |
| $K_2Al_{10}Methyl_{10}$ | | -0.0105 | |
| $Al_{13}Na$ | -0.0001 | -0.0017 | 0.0092 |
| $Al_{12}Na_3$ | -0.0092 | -0.0042 | 0.0115 |
| $Al_{12}Mg$ | -0.0002 | -0.0056 | 0.0043 |
| $Al_{12}Mg_3$ | -0.0013 | -0.0030 | 0.0060 |

*Table 1 – Laplacian at different critical points*

These values show that in bonds between aluminum and a dopant atom, both sodium and magnesium have positive Laplacians of the charge density at the critical point. However, sodium tends to have a more positive Laplacian, suggesting that it behaves more ionically than magnesium. We see that the Al-Al bonding is characterized by either a positive or negative value depending on the cluster. In an Aluminum-Methyl cluster the Laplacian of the charge density between two aluminum atoms was -0.0105, which marks a covalent bond. Conversely, in $Al_{13}^-$, the Laplacian was +0.0065, indicating an ionic bond. This shows that, like the dipole moment, the Laplacian of the charge density is not a suitable metric in distinguishing between metallic and ionic bonding.

### 3.6 Mulliken Population

The Mulliken population is based on how occupied the individual atomic orbitals are. A sodium atom has a single 3s electron, while magnesium has a pair; the 3p orbitals of both are unoccupied. In an ionic bond, we would expect the 3s occupation of the dopant to be negligible

since the electrons are being transferred to some anion. Figure 13 shows the average Mulliken population of the 3s and 3p orbitals in the dopant atoms as a function of cluster size.

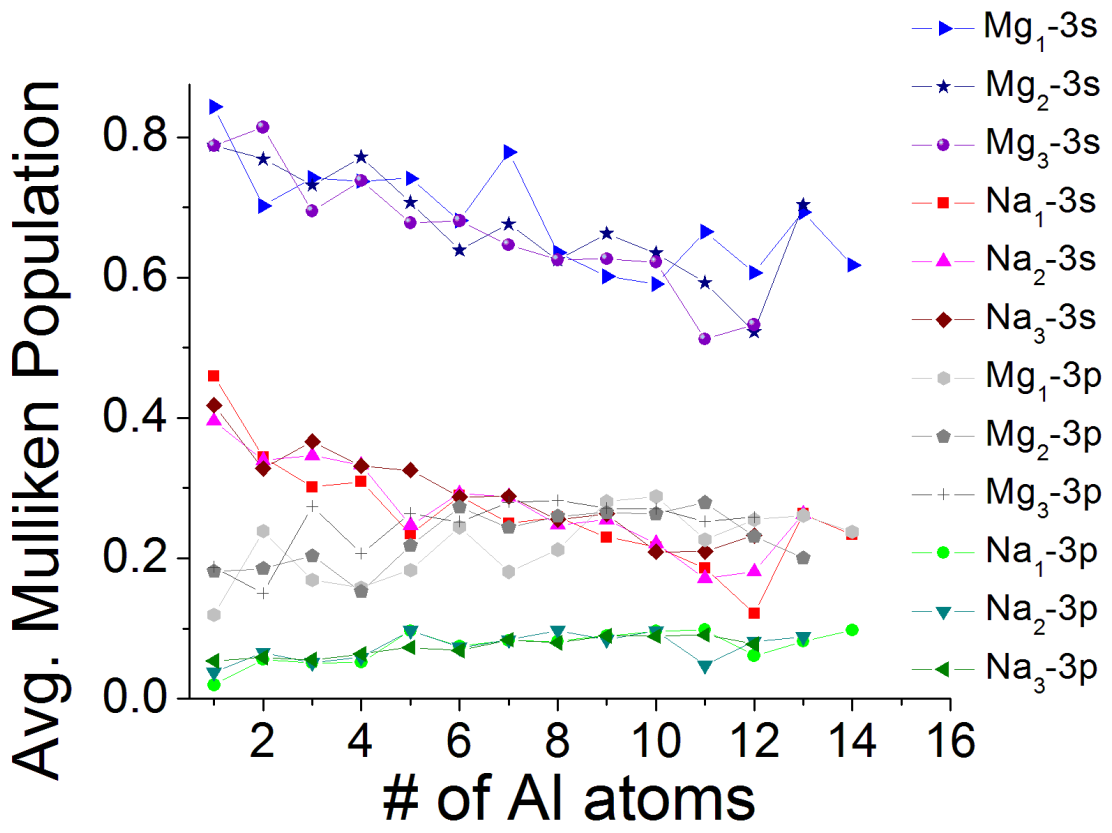


*Figure 13 – Average 3s and 3p Mulliken population for $Al_mNa_n$ and $Al_mMg_n$.*

These results show that the 3s occupation in magnesium is higher than the 3s occupation in sodium for clusters of the same size. In both cases, the 3s occupation decreases as the size as the cluster gets larger. The 3p occupation of sodium remains negligible, while the 3p occupation of the magnesium increases with cluster size. In fact, at cluster containing more than eight aluminum atoms, the 3p occupation of magnesium exceeds the 3s occupation of sodium in clusters of the same size. The small occupation of the sodium orbitals is in agreement with the Hirshfeld charge analysis; sodium tends to more easily donate its electron to the aluminum motif. The occupation of the 3p orbital is an important marker in determining metallic bonding. It's

been shown in pure magnesium clusters, that occupation of the 3p orbital is indicative of a metallic transition. In this series, we see that the 3p orbital for the magnesium does increase, while the 3p occupation in the sodium atoms remain negligible. In spite of the fact that magnesium normally has an unoccupied 3p subshell, something is causing this subshell to become energetically favorable. This result suggests that Mulliken occupation of the valence p subshell can be used to quickly characterize bonding in group I and II elements.

### 3.7 Change in removal energy

The change in removal energy ($\Delta E_{R.E}$) of the dopant between its neutral and anionic clusters can be used to distinguish between metallic and ionic bonding. Ionic bonds are stabilized first by electronic transfer, and then reinforced by a Coulombic attraction between the cation and anion. If an extra electron is added (as is the case in an anionic cluster), we would expect an ionic bond to become destabilized since the presence of an extra electron would decrease the electronic transfer. For this reason, we calculated the difference in dopant removal energies between the neural and anionic species.

$$\Delta E_{R.E.} = [\text{dopant removal energy - Anion}] - [\text{dopant removal energy - Neutral}]$$

If this quantity is negative, the energy with which the dopant was bound decreases when an additional electron is added, which indicates an ionic bond. If the change in removal energy is positive, the extra electron stabilizes the bond, suggesting the bond is not ionic. Figure 14 shows the change in removal energy for the sodium and magnesium series.

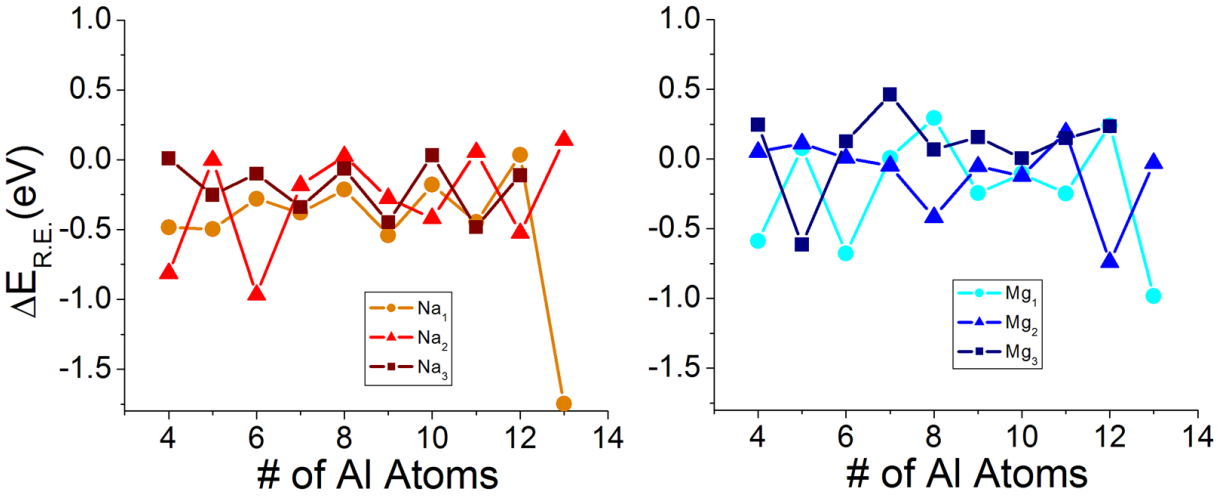


*Figure 14 - Change in dopant removal energy in $Al_mNa_n^-$ and $Al_mMg_n^-$ versus $Al_mNa_n$ and $Al_mMg_n$*

The bond that sodium makes with the aluminum motif is always destabilized by the addition of an electron, with only a few exceptions whose difference was always less than 0.2 eV. The magnesium series does not possess a clear trend. The extra electron acted to stabilize the bond as often as it acted to destabilize it. This reinforces the idea that magnesium is less ionic than sodium.

### 3.8 Change in Electronic Structure

The final metric to be examined is the comparison of the electronic structure of an optimized bimetallic system, a single point calculation of that same system as an anion with the dopant atoms replaced with the corresponding number of electrons, and an optimized calculation of that anionic system. If the dopants are ionically bound to the aluminum motif, there should be little difference among the bimetallic system, and the unoptimized and optimized anionic systems. First, we investigate $Al_{12}Na^-$. The electronic structures of this cluster, a single point calculation

of the geometry without the sodium and with an extra electron, and an optimized calculation of that anionic species. Figure 15 shows that these three systems have very similar electronic structures.

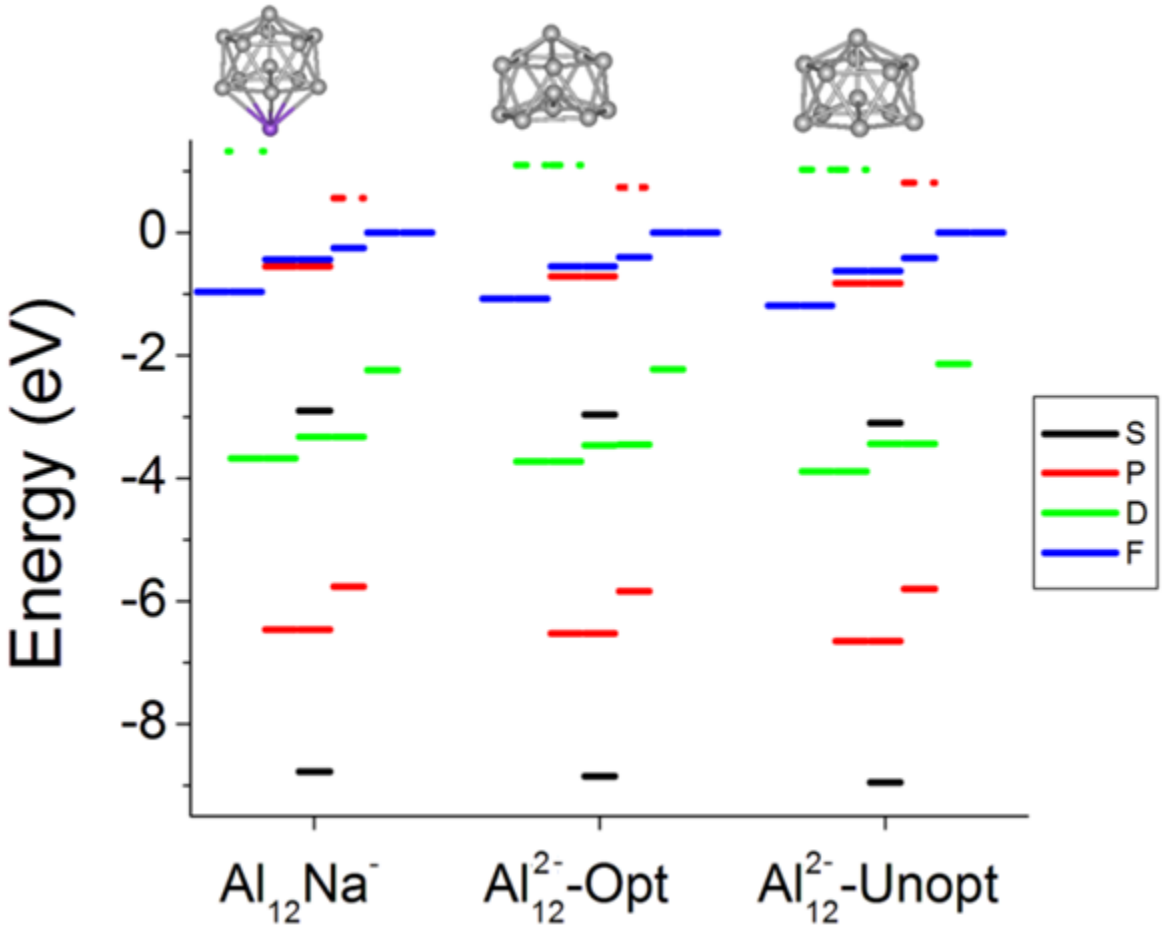


*Figure 15 - Electronic structures of $Al_{12}Na^-$*, an $Al_{12}^{-2}$ optimized, and unoptimized $Al_{12}^{-2}$ structure based on $Al_{12}Na^-$

This demonstrates that the $Al_{12}Na^-$ cluster possess a very similar electronic structure as $Al_{12}^{2-}$, and that the primary role of the sodium in this system is to donate an electron to the aluminum motif.

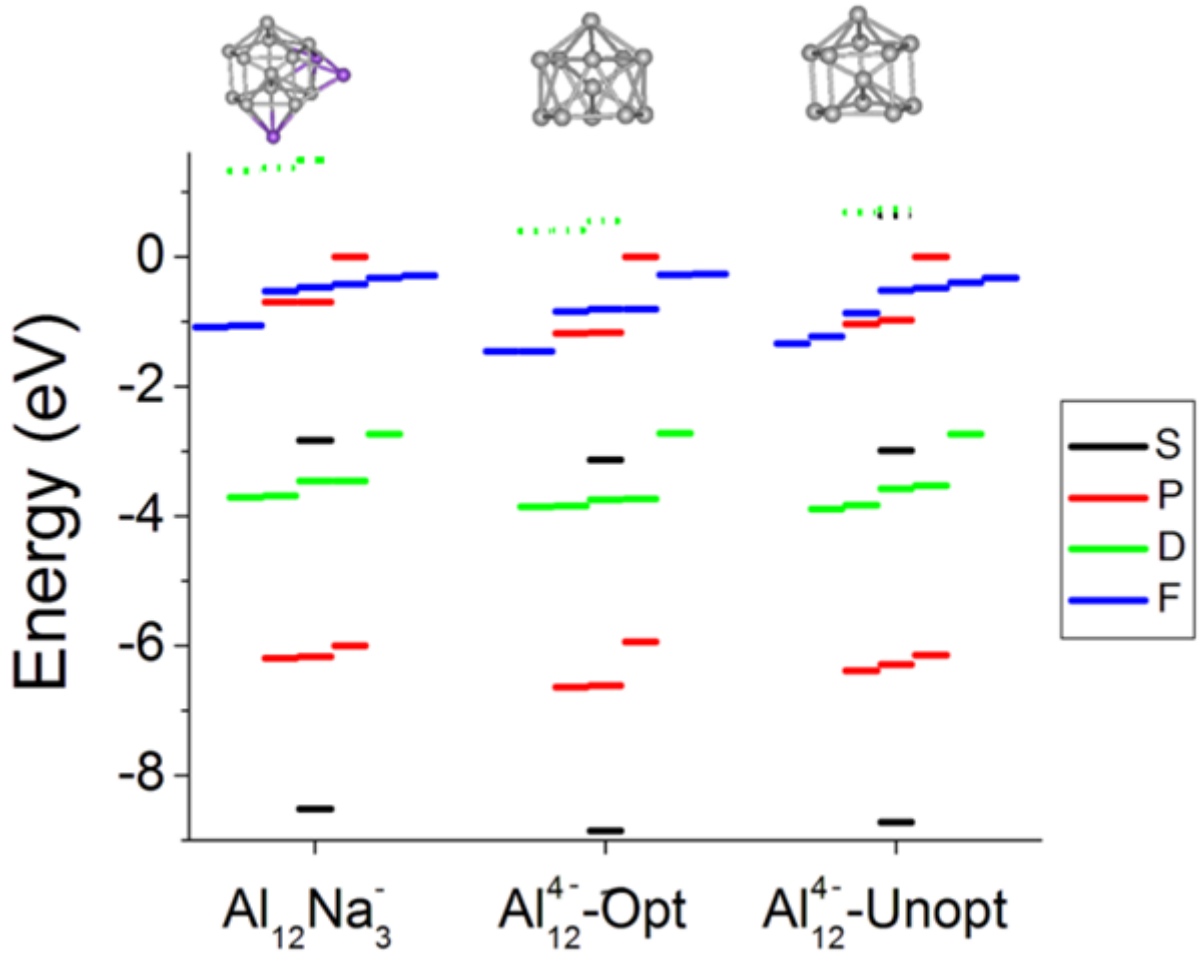


*Figure 16 - Electronic structures of $Al_{12}Na_3^-$, an $Al_{12}^{4-}$ optimized, and unoptimized $Al_{12}^{4-}$ structure based on $Al_{12}Na_3^-$*

Next, we investigate the role of sodium in $Al_{12}Na_3^-$. Again, the three electronic plots shown in Figure 16 correspond to the optimized $Al_{12}Na_3^-$, a single point calculation of this geometry with the sodium atoms replaced with their corresponding electrons, and an optimized $Al_{12}^{4-}$ cluster. Again, the three electronic plots are similar. The major differences among the three plots are subshells losing their degeneracy. This is a result of the optimized $Al_{12}^{4-}$ being more symmetrical than the other two systems. These results again show that the primary contribution of the sodium atoms to these clusters is the donation of its electrons.

Finally, we repeat this process with $Al_{11}Mg_3^-$. Because magnesium is divalent, the corresponding anion will have two extra electrons per magnesium atom. Figure 17 shows the electronic plots of $Al_{11}Mg_3^-$, a single point calculation on $Al_{11}^{7-}$, where the geometry matches the aluminum motif from $Al_{11}Mg_3^-$, and an optimized $Al_{11}^{-7}$.

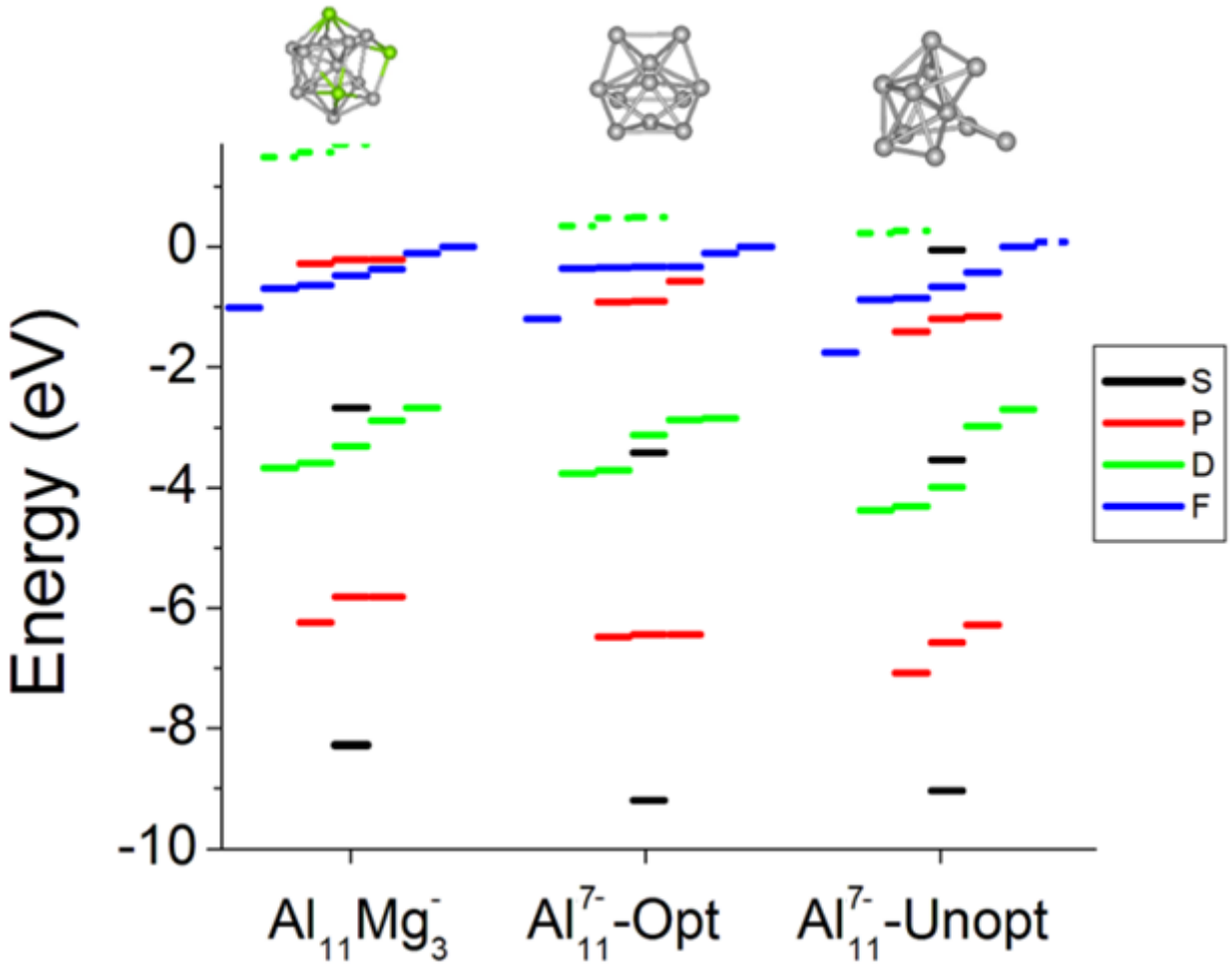


*Figure 17 - Electronic structures of $Al_{11}Mg_3^-$, an $Al_{11}^{-7}$ optimized, and unoptimized $Al_{11}^{-7}$ structure based on $Al_{11}Mg_3^-$*

Unlike the sodium systems which was isoelectric in all three calculations, this plot shows a rearrangement in the order of the electronic states. The crystal field splitting in the single point calculation on $Al_{11}^{7-}$ is so dramatic that one of the 1F orbitals because unoccupied while the 3S

orbital becomes filled. This cluster has a HOMO-LUMO gap of 0.08eV. The reordering of the electronic structure among the three calculations, along with the dramatic change in calculated HOMO-LUMO gap (which was 1.45eV in the bimetallic cluster), show that the presence of magnesium affects the electronic structure more than the presence of its electrons.

# Chapter 4

# Nature of Bonding in Ligated Aluminum Clusters

## 4.1 Introduction

The Jellium model can be used to describe the formation of high HOMO-LUMO gaps in magnesium/sodium doped aluminum clusters possessing "magic numbers" of electrons. These electron counts correspond to closing of electronic shells, similar to those found in atomic systems. As the geometry of the clusters shifts from spherical to prolate or oblate, crystal field splitting occurs within the subshells allowing for a high HOMO-LUMO gap in electron counts not corresponding to "magic numbers". Conceptually, the spherical Jellium model is metallic in nature; the electrons exist as a free gas in a uniform and continuous positive background charge.

In contrast, Wade-Mingos rules describe polyhedral systems where atomic *p* orbitals form cage bonds that act to stabilize the shell. This model has been applied to describe tin, lead, and germanium clusters, as well as the unexpected stability of, $Al_4H_6$, all of which possess a closo-structure. In this cluster, each Al-H subunit possess one electron pair available for bonding, and the extra to hydrogen provide another. In this section, the ground state geometries of aluminum-

methyl clusters are calculated and their electronic structures analyzed. Similar to $Al_4H_6$, each aluminum-methyl subunit (AlMe) has one electron pair available for bonding. These aluminum-methyl clusters were modeled with two potassium atoms, which provided the extra electron pair required for a closo-structure.

## 4.2 Structure

By assuming the two potassium atoms as donating their electrons to the aluminum-methyl cage, this system $(AlMe)_n^{-2}$ can be considered to be analogous to borane $B_nH_n^{-2}$. Each aluminum-methyl subunit has ten valence electrons. One electron from each of the hydrogens, three from the aluminum, and four from the carbon. Six of the electrons are required for the three C-H bonds in the methyl, and two more are required for the Al-C bond. This leaves one electron pair per vertex. With the extra electron pair form the potassium atoms, the number of bonding pairs of electrons is equal to (n+1), or (2n+2) electrons, which implies closo-structures. The ground state geometries for $K_2(AlMe)_n$ are shown in Figure 18. The brown atoms forming a cage-like structure are aluminum. The ligands associated with each of the aluminum atoms is a methyl ($CH_3$). The purple atoms are potassium.

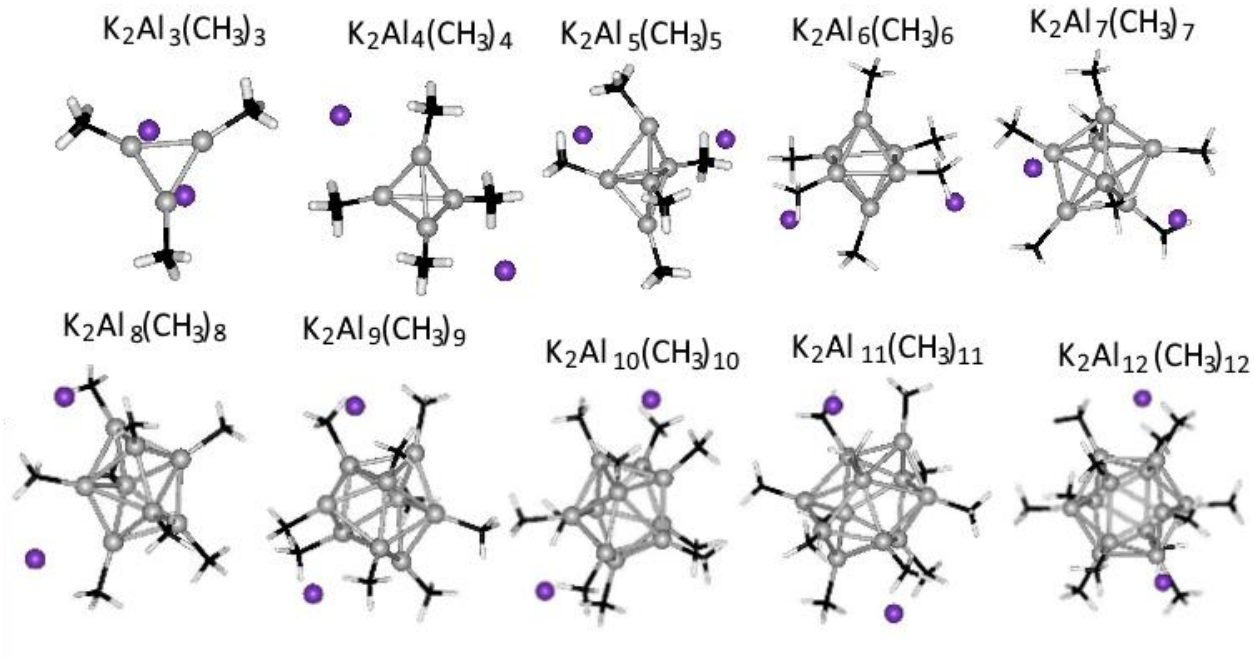


*Figure 18 - Ground state geometry of $K_2Al_nMe_n$*

In all cases, the aluminum atoms form cage structure, with both potassium atoms tending to appear on the same side of the cluster, but not adjacent to one another. In spite of the symmetry of all clusters being disrupted by the potassium ions, the aluminum cages are consistent with the structures predicted by Wade-Mingos rules.

### 4.3 HOMO-LUMO gap and Removal Energies

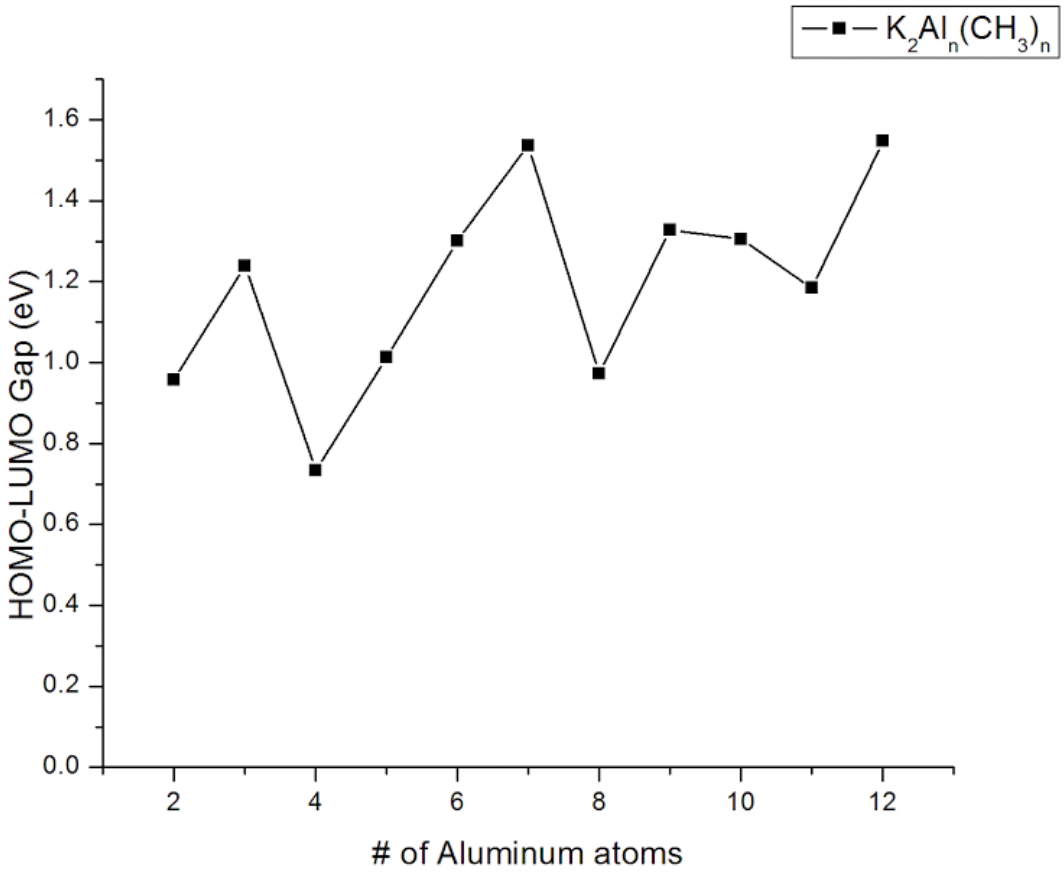


*Figure 19 - HOMO-LUMO Gaps of $K_2(AlMe)_n$*

The HOMO-LUMO gap for these clusters can be found in Figure 19. With the exception of $K_2(AlMe)_4$, all clusters possessed a high HOMO-LUMO gap (0.97 eV – 1.6 eV). There are local maxima at n = 7 and n=12, where the HOMO-LUMP gap is greater than 1.5 eV There are local minima at n = 4 and 8, where the gap is 0.73 eV and 0.97 eV. Dodecaborane, $B_{12}H_{12}^{2-}$, was also modeled to provide a comparison for a known Wade-Mingos cluster. The HOMO-LUMO gap of this cluster was calculated to be 5.39eV, substantially higher than any of the clusters investigated.

This result is completely different than those from the bimetallic clusters previously investigated, where only certain "magic numbers" of electrons would lead to a high HOMO-LUMO gap. In the bimetallic clusters, oscillations are observed in the HOMO-LUMO gap between even and odd numbers of aluminum atoms. This is due to the fact that aluminum has three valence electrons, so the number of electrons switches between even and odd when an aluminum is added. Clusters with odd numbers of electrons tend to have lower HOMO-LUMO gaps, since these clusters will have an unpaired electron. Because each aluminum-methyl subunit has ten valence electrons, all clusters contain an even number of electrons. The high HOMO-LUMO gap for all clusters, along with the calculated structures, show that this system is best modeled using Wade-Mingos counting rules and not the Jellium model.

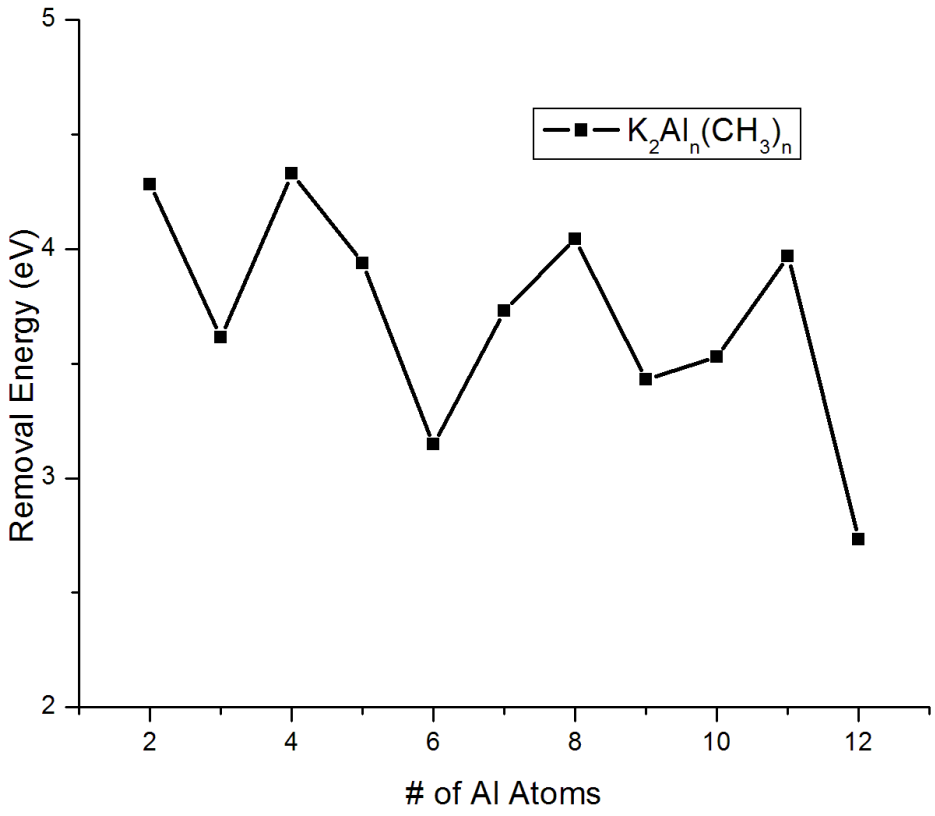


*Figure 20 - AlMe Removal energy in K2(AlMe)$_n$ clusters*

Figure 20 shows the energy required to remove an aluminum-methyl subgroup as a function of cluster size. The removal energy of the aluminum-methyl subgroup stays between 2.8 eV and 4.2 eV, with local minima at n = 4, 8, and 11. The lowest removal energy occurs in the n = 12 clusters. These values are much lower than the removal energy of a BH unit from $B_{12}H_{12}^{2-}$.

### 4.4 Mulliken Population

In the previous section, we used the Mulliken population in our investigation of the nature of bonding between aluminum clusters and the dopants. In this chapter, we use this parameter to investigate any difference between pure aluminum clusters, and the ligated aluminum clusters. The average Mulliken population of aluminum orbitals are plotted as a function of cluster size for pure neutral aluminum clusters and ligated clusters. Figure 21 shows these Mulliken populations.

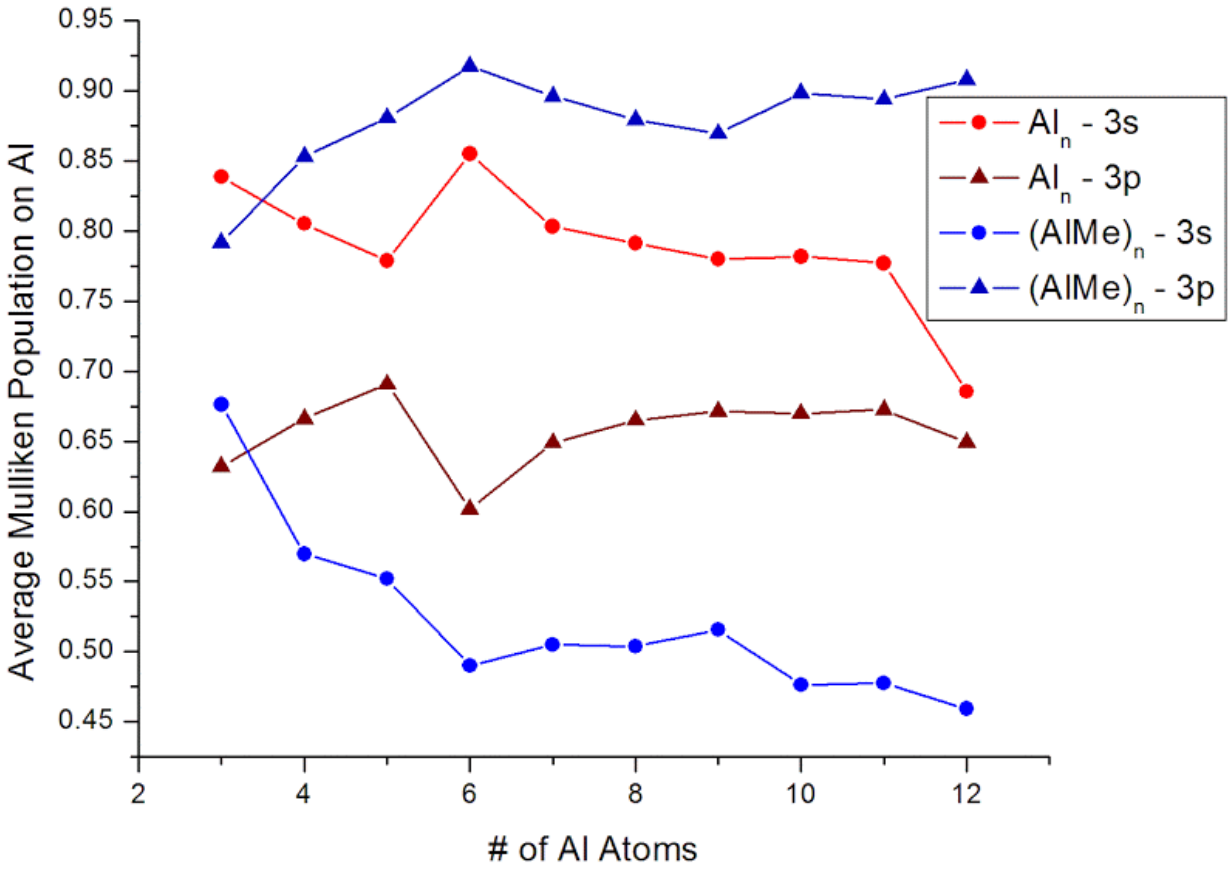


*Figure 21 - Mulliken population of pure aluminum clusters and ligated clusters*

The two red traces refer to the neutral pure aluminum clusters, while the blue traces correspond to the ligated aluminum clusters. The trace that is lighter in color with circle markers is the 3*s*

occupation, while the darker trace with the triangular markers display the 3*p* occupation. This shows a clear difference between the two systems. In pure aluminum clusters, the 3*s* occupation is higher than the 3*p* occupation. Conversely, in the ligated clusters, the 3*p* occupation is much higher than the 3*s* occupation. Wade-Mingos counting rules operates on the principle that the atomic *p* orbitals overlap to form delocalized molecular orbitals. In the following section, we investigate the electronic structures for the ligated aluminum clusters.

## 4.5 Electronic Structure

The electronic structures of these clusters were analyzed to confirm whether the high HOMO – LUMO gap can be explained with Wade-Mingos counting rules.

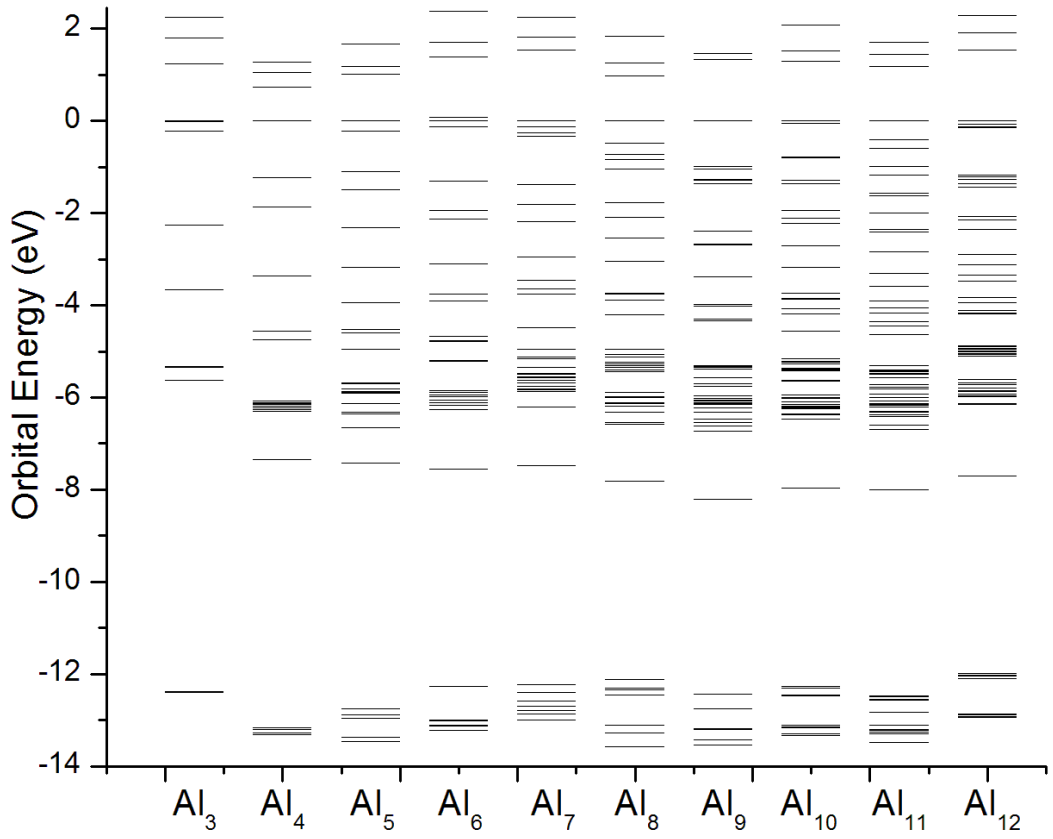


*Figure 22 - Electronic stucture of $K_2(AlMe)_n$ ($3 \leq n \leq 12$).*

Figure 22 shows the electronic energies for $K_2(AlMe)_n$ ($3 \leq n \leq 12$). The energies of all orbitals for each species were shifted such that the highest occupied molecular orbital corresponded to 0 eV. Investigating the shape of the individual orbitals, showed a common pattern among the clusters. For a given cluster $K_2(AlMe)_n$, there were *n* states that were very energetically favorable that corresponded to the bonding between hydrogen and carbon in the methyl groups. There were then *n* states corresponding to bonds between the aluminum and carbon atoms, with a high amount of crystal field splitting among these states. Within this range, there were 2*n* additional orbitals corresponding to bonding between hydrogen and carbon in the methyl groups. There was then a unique orbital that was visually similar to the 3S atomic orbital. The highest *n* orbitals

corresponded to bonding among the aluminum atoms in the cage, where the bonds appeared to have *p* shell characteristics.

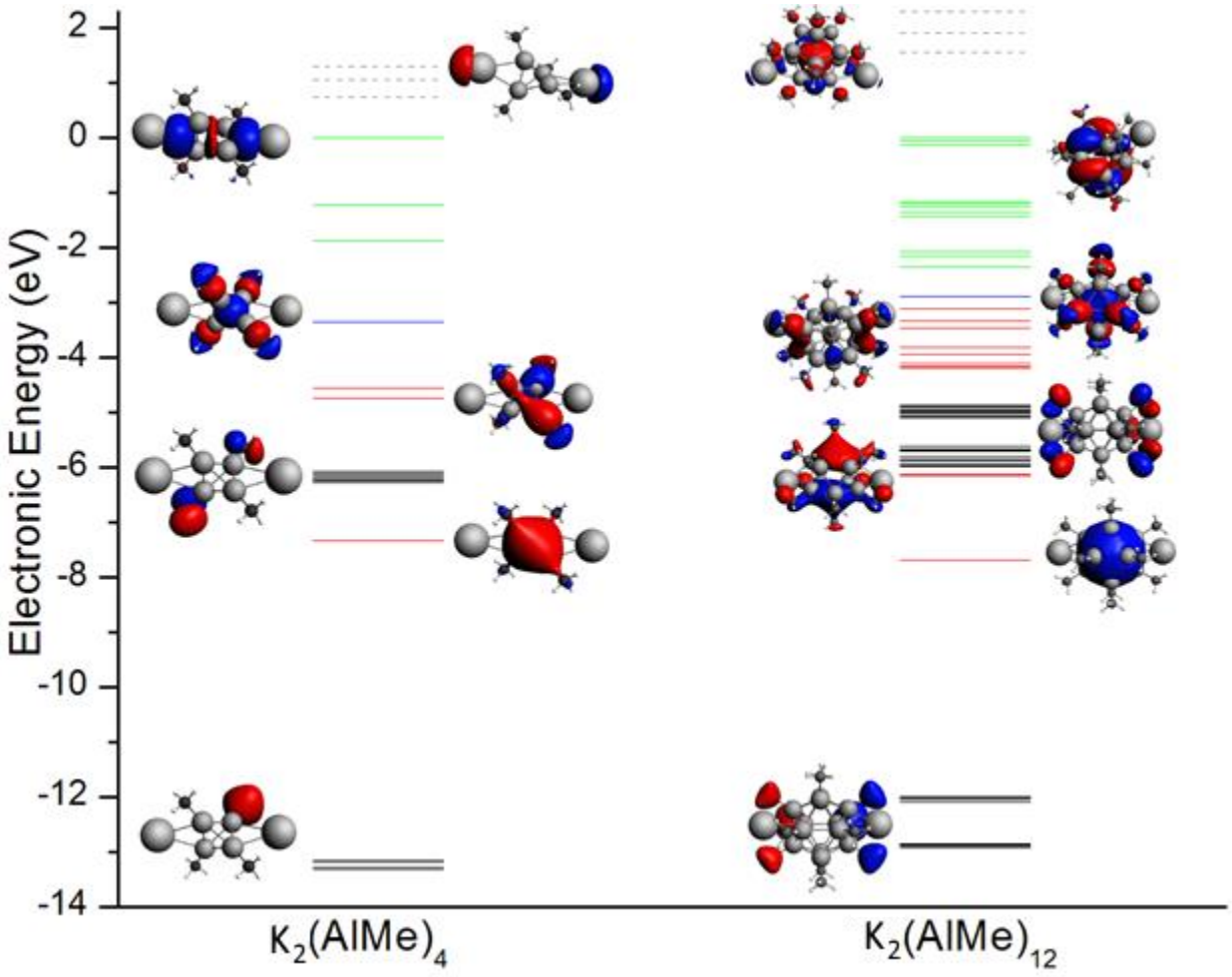


*Figure 23 - Electronic Structure of $K_2(AlMe)_4$ and $K_2(AlMe)_{12}$*

Figure 23 shows the electronic structure of $K_2(AlMe)_4$ and $K_2(AlMe)_{12}$. The colors of the energy levels are based on characterization of the orbitals. Black lines represent orbitals located on the methyl groups. There are *3n* such orbitals for each structure. Red represents bonding between the carbon and aluminum that possesses S-type characteristics (*n* orbitals in each cluster). The blue line represents the single unique orbital that visually similar to a 3S type orbital. Green represents bonding between the carbon and aluminum that possesses P-type characteristics (*n*

orbitals in each cluster). This plot shows that the presence of the potassium atoms splits the orbitals, leading to lower HOMO-LUMO gap compared to $Al_4Me_4^{2-}$. The pattern for the electronic structure is the same for each species studied.

# Chapter 5

# Conclusion and Future Work

## 5.1 Conclusion and Future Work

This study shows that sodium and magnesium bind differently to aluminum. Sodium tends to have low Mulliken populations in its 3*s* and 3*p* orbitals, and high Hirshfeld charges, Laplacian of the charge density, and dipole moment. The change in removal energy between neutral and anionic species show that its bond with the aluminum motifs becomes destabilized with the addition of an electron. Finally, the electronic structures of $Al_{12}Na^-$ and $Al_{12}Na_3^-$ were closely modeled by replacing the sodium atoms with their corresponding electrons. With these results, we can conclude that sodium forms ionic bonds in bimetallic clusters with aluminum.

The behavior of magnesium is not as obvious as sodium. It tended to donate a smaller amount of charge compared to sodium in clusters of the same size, and in turn induced a smaller dipole. Its 3*p* Mulliken population increased with cluster size, while its 3*s* occupation decreased. There was no clear tread showing an extra electron would destabilize its bond with. The tendency of magnesium to embed itself within the aluminum motif caused the electronic structure of $Al_{11}Mg_3^-$ to be very different than $Al_{11}^{7-}$. These results suggest that the way magnesium bonds to aluminum can be considered metallic.

Of the parameters investigated, the Mulliken population of the dopants serves as the best indication of the nature of bonding since it yields useful information without requiring an additional calculation. In clusters with multiple dopants, the net electric dipole can be minimized by symmetric spacing of the dopants. Measuring the change in removal energy between a neutral and anionic cluster of the same composition, as well as investigating the change in electronic structure if the dopants are replaced with the corresponding number of valence electrons, requires extra calculation.

We have also investigated the ground state and electronic structures of $K_2(AlMe)_n$ ($3 \leq n \leq 12$). Because each aluminum-methyl sub group has one electron pair available for skeletal bonding, we expect this system to be best described with Wade-Mingos counting rules. Our calculated structures were consistent with the closo-structures predicted by this model. We found that all species in the series possessed a high HOMO-LUMO gap, further suggesting that the system conformed to the Wade-Mingos picture. The Mulliken population showed that the occupation of the atomic orbitals was fundamentally different between pure and ligated aluminum clusters. The ligated aluminum cluster had a much higher 3*p* occupation, which is indicative that Wade-Mingos rules are applicable. By investigating the electronic structure, we showed that a pattern emerged that is consistent with Wade-Mingos counting rules.

This study demonstrates that the properties of a cluster can be dramatically different than the properties of the constituent elements. We showed that aluminum can bind metallically or covalently depending on the other elements in the cluster. This versatility is why clusters are being investigated as building blocks for cluster assembled materials: the properties of a cluster is highly dependent on its size as well as its composition.

# References


[1] N.K. Chaki, S. Mandal, A.C. Reber, M. Qian, H.M. Saavedra, P.S. Weiss, S.N. Khanna, and A. Sen, ACS Nano **4**, 5813 (2010).

[2] S.A. Claridge, A.W. Castleman, S.N. Khanna, C.B. Murray, A. Sen, and P.S. Weiss, ACS Nano **3**, 244 (2009).

[3] A.W. Castleman, S.N. Khanna, A. Sen, A.C. Reber, M. Qian, K.M. Davis, S.J. Peppernick, A. Ugrinov, and M.D. Merritt, Nano Lett **7**, 2734 (2007).

[4] A.W. Castleman and S.N. Khanna, J Phys Chem C **113**, 2664 (2009).

[5] S.N. Khanna and P. Jena, Phys. Rev. B **51**, 13705 (1995).

[6] R.E. Leuchtner, A.C. Harms, and A.W. Castleman, J. Chem. Phys. **94**, 1093 (1991).

[7] M. Qian, A.C. Reber, A. Ugrinov, N.K. Chaki, S. Mandal, H.M. Saavedra, S.N. Khanna, A. Sen, and P.S. Weiss, ACS Nano **4**, 235 (2009).

[8] S.N. Khanna and P. Jena, Chem. Phys. Lett. **219**, 479 (1994).

[9] P. Jena, S. n. Khanna, and B. k. Rao, Surf. Rev. Lett. **03**, 993 (1996).

[10] J. Akola, M. Manninen, H. Häkkinen, U. Landman, X. Li, and L.-S. Wang, Phys. Rev. B **62**, 13216 (2000).

[11] Z. Luo, C.J. Grover, A.C. Reber, S.N. Khanna, and A.W. Castleman, J. Am. Chem. Soc. **135**, 4307 (2013).

[12] H. Häkkinen and U. Landman, Phys. Rev. B **62**, R2287 (2000).

[13] A. Nakajima, K. Hoshino, T. Naganuma, Y. Sone, and K. Kaya, J. Chem. Phys. **95**, 7061 (1991).

[14] A.C. Reber, S.N. Khanna, P.J. Roach, W.H. Woodward, and A.W. Castleman, J Am Chem Soc **129**, 16098 (2007).

[15] S. Mandal, A.C. Reber, M. Qian, P.S. Weiss, S.N. Khanna, and A. Sen, Acc. Chem. Res. **46**, 2385 (2013).

[16] M. Brack, Rev. Mod. Phys. **65**, 677 (1993).

[17] W. Ekardt, Phys. Rev. B **29**, 1558 (1984).

[18] K. Wade, J. Chem. Soc. Chem. Commun. 792 (1971).

[19] D.M. P. Mingos, J. Chem. Soc. Chem. Commun. **0**, 706 (1983).

[20] H. Schäfer, B. Eisenmann, and W. Müller, Angew. Chem. Int. Ed. Engl. **12**, 694 (1973).

[21] R. Hoffmann, Angew. Chem. Int. Ed. Engl. **26**, 846 (1987).

[22] L.C. Allen and J.F. Capitani, J. Am. Chem. Soc. **116**, 8810 (1994).

[23] H.-J. Zhai, B. Kiran, J. Li, and L.-S. Wang, Nat. Mater. **2**, 827 (2003).

[24] A.C. Reber and S.N. Khanna, J. Chem. Phys. (2015).

[25] W.D. Knight, K. Clemenger, W.A. de Heer, W.A. Saunders, M.Y. Chou, and M.L. Cohen, Phys. Rev. Lett. **52**, 2141 (1984).

[26] Z. Luo, G.U. Gamboa, J.C. Smith, A.C. Reber, J.U. Reveles, S.N. Khanna, and A.W. Castleman, J. Am. Chem. Soc. **134**, 18973 (2012).

[27] F.L. Hirshfeld, Theor. Chim. Acta **44**, 129 (1977).

[28] R.S. Mulliken, J. Chem. Phys. **3**, 375 (1935).

[29] J.P. Perdew, K. Burke, and M. Ernzerhof, Phys. Rev. Lett. **77**, 3865 (1996).

[30] J. Akola, K. Rytkönen, and M. Manninen, Eur. Phys. J. - At. Mol. Opt. Plasma Phys. **16**, 21 (2001).

[31] O. Kostko, B. Huber, M. Moseler, and B. von Issendorff, Phys. Rev. Lett. **98**, 043401 (2007).

[32] G. te Velde, F.M. Bickelhaupt, E.J. Baerends, C. Fonseca Guerra, S.J.A. van Gisbergen, J.G. Snijders, and T. Ziegler, J. Comput. Chem. **22**, 931 (2001).

[33] E. Van Lenthe and E.J. Baerends, J. Comput. Chem. **24**, 1142 (2003).